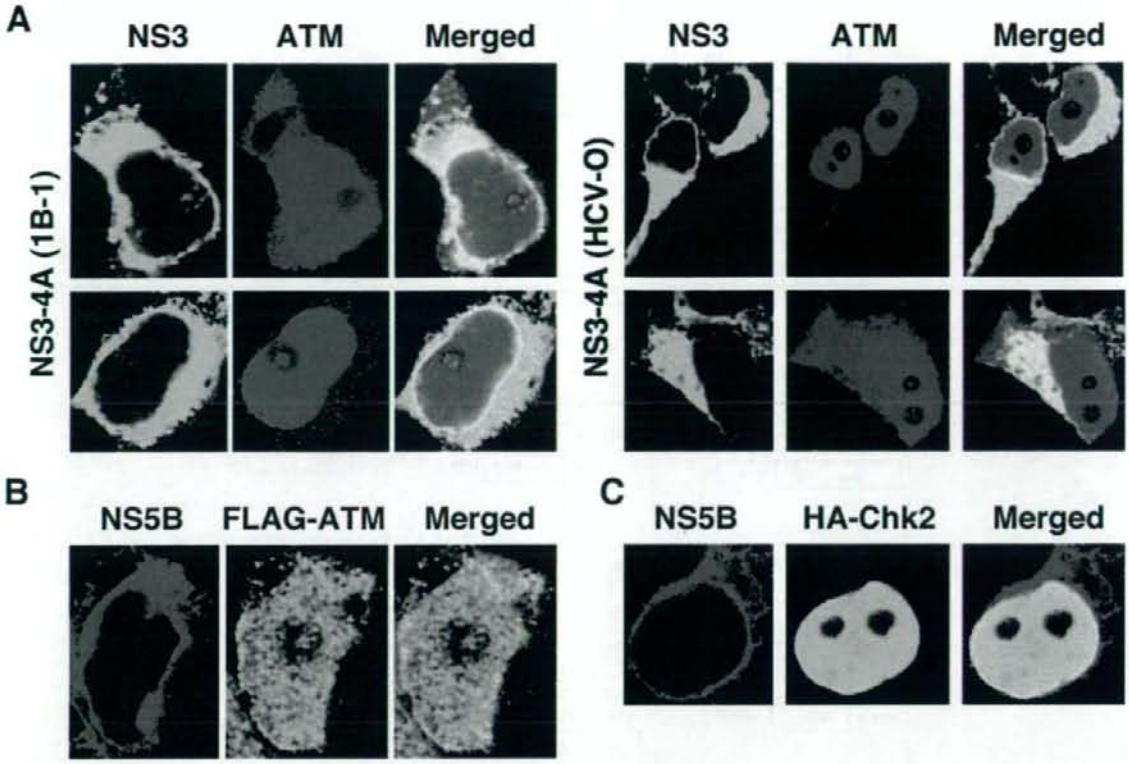

FIG. 5. Subcellular localization of ATM and Chk2 in HCV NS3-4A- or NS5B-expressing cells. (A) ATM partially colocalized with HCV NS3-4A. 293FT cells cotransfected with 300 ng of pCX4bsr/NS3-4A (1B-1) (8) or pCX4bsr/NS3-4A (O) (8) and 300 ng of pcDNA3-FLAG-ATMwt (6) were examined by confocal laser scanning microscopy. Cells were stained with anti-NS3 and anti-ATM (5C2) antibodies and then visualized with FITC (NS3) or Cy3 (ATM). (B) ATM partially colocalized with HCV NS5B. 293FT cells cotransfected with 300 ng of pCX4bsr/NS5B (1B-1) (23) and 300 ng of pcDNA3-FLAG-ATMwt (6). Cells were stained with anti-NS5B (no. 14) and anti-ATM (PM026) antibodies and then visualized with FITC (ATM) or Cy3 (NS5B). (C) Chk2 partially colocalized with HCV NS5B. 293FT cells cotransfected with 300 ng of pCX4bsr/NS5B (1B-1) (23) and 300 ng of pcDNA3-HA-Chk2wt (20, 21). Cells were stained with anti-NS5B and anti-HA (3F10) antibodies and then visualized with FITC (HA-Chk2) or Cy3 (NS5B). Images were visualized using confocal laser scanning microscopy (LSM510; Carl Zeiss). The right panels exhibit two-color overlay images (Merged). Colocalization is shown in yellow.

useful for the clinical treatment of patients with chronic hepatitis C.

Interaction of HCV NS3-4A with ATM. Since HCV NS3 has been proposed to be a viral factor involved in the induction of dsDNA breaks (18, 19), we first examined the subcellular localization of NS3-NS4A ([NS3-4A] 1B-1 or HCV-O strain) and ATM by confocal laser scanning microscopy. In most of the observed cells, ATM partially colocalized with NS3-4A in the perinuclear region and in dispersed points throughout the cytoplasm (Fig. 5A). In particular, we observed prominent colocalization of ATM with NS3-4A in some cells (Fig. 5A). Next, using anti-FLAG and anti-ATM antibodies, we immunoprecipitated lysates from 293FT cells in which FLAG-tagged ATM and either NS3-4A (HCV-O) or NS3 (HCV-O) were overexpressed and then performed immunoblotting analysis using either anti-ATM or anti-NS3 antibody to determine whether ATM binds to NS3-4A or NS3. The results revealed that ATM preferentially bound to NS3-4A over NS3 alone (Fig. 6A). Similarly, we found that ATM bound to NS3-4A using the O cell lysates (Fig. 6B), while HA-tagged Chk2 did not bind to NS3-4A in immunoprecipitation analysis using lysates from 293FT cells in which NS3-4A and HA-tagged Chk2 were overexpressed (Fig. 6C). Although NS3-4A has protease activity, ATM was not cleaved by the NS3-4A protease (Fig. 6D). Taking these results together, we conclude that ATM is able to interact with NS3-4A.

Interaction of HCV NS5B with ATM and Chk2. We next examined the subcellular localization of ATM and/or Chk2 in HCV NS5B-expressing cells by confocal laser scanning microscopy since we previously demonstrated that HCV NS5B-expressing PH5CH8 immortalized human hepatocyte cells were susceptible to DNA damage in the form of dsDNA breaks (23). ATM partially colocalized with NS5B in dispersed points throughout the cytoplasm (Fig. 5B), similar to the subcellular localization of HCV NS3-4A and ATM. Furthermore, Chk2 also partially colocalized with NS5B in the perinuclear region and in dispersed points in the nucleus (Fig. 5C). To determine whether endogenous ATM binds to NS5B, lysates from Oc or

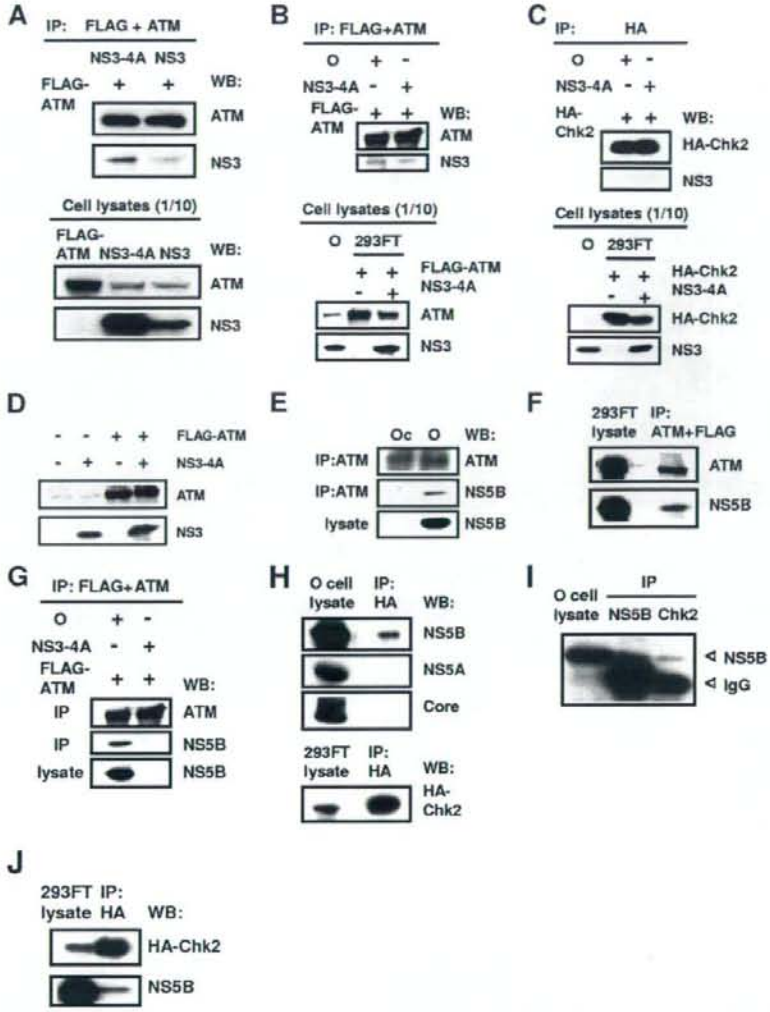

FIG. 6. Interaction of HCV NS3-4A and NS5B with the ATM signaling pathway. (A and B) ATM bound to HCV NS3-4A. (A) 293FT cells were transfected with 4 μg of pCX4bsr/NS3-4A (O), 4 μg of pCX4bsr/NS3 (O), or 4 μg of pcDNA3-FLAG-ATMwt. The cell lysates of expressed FLAG-ATM were mixed with lysates expressing either NS3-4A or NS3. The cell lysates were immunoprecipitated with both anti-FLAG (M2) and anti-ATM (2C1) antibodies, followed by immunoblotting analysis using either anti-ATM (2C1) or anti-HCV NS3 antibody. The results of Western blot analysis of 1/10 of the cellular lysates with anti-ATM or anti-NS3 antibody are also shown. (B) 293FT cells were cotransfected with 4 μg of pcDNA3-FLAG-ATMwt and/or 4 μg of pCX4bsr/NS3-4A (O). The cell lysates of expressed FLAG-ATM alone were mixed with the O cell lysates. Immunoprecipitation and Western blot analysis were performed as described in panel A. (C) Chk2 did not bind to NS3-4A. 293FT cells were cotransfected with 4 μg of pcDNA3-HA-Chk2wt and/or 4 μg of pCX4bsr/NS3-4A (O). The cell lysates of expressed HA-Chk2 alone were mixed with the O cell lysates. The cell lysates were immunoprecipitated with anti-HA antibody (3F10), followed by Western blot analysis using either anti-HA (HA-7) or anti-HCV NS3 antibody. The results of Western blot analysis of 1/10 of the cellular lysates with anti-HA or anti-NS3 antibody are also shown. (D) ATM was not cleaved by HCV NS3-4A protease. 293FT cells were cotransfected with 4 μg of pCX4bsr/NS3-4A (O) and/or 4 μg of pcDNA3-FLAG-ATMwt. The results of Western blot analysis of cellular lysates with anti-ATM or anti-NS3 antibody are shown. (E to G) ATM bound to HCV NS5B. (E) The lysates of O or Oc cells were immunoprecipitated with anti-ATM antibody (2C1), followed by immunoblotting analysis using either anti-ATM or anti-HCV NS5B antibody (no. 14). The results of Western blot analysis of 1/10 of the cellular lysates with anti-NS5B antibody are also shown. (F) 293FT cells were cotransfected with 4 μg of pCX4bsr/NS5B (1B-1) and 4 μg of pcDNA3-FLAG-ATMwt. The cell lysates were immunoprecipitated with both anti-FLAG and anti-ATM antibodies, followed by immunoblotting analysis using either anti-ATM or anti-HCV NS5B antibody. (G) Western Blot analysis was performed with anti-NS5B antibody, reusing the same blotted membrane that was used for panel B. (H to J) Chk2 bound to HCV NS5B. (H) 293FT cells were cotransfected with 4 μg of pcDNA3-HA-Chk2wt. The cell lysates of expressed HA-Chk2 were mixed with the O cell lysates and were immunoprecipitated with anti-HA antibody (3F10), followed by immunoblotting analysis using anti-HCV NS5B, anti-HCV NS5A (no. 8926), anti-HCV core protein (CP-9 and CP-11 mixture), or anti-HA (HA-7) antibody. The results of Western blot analysis of 1/10 of the cellular lysates with the same antibodies are also shown. (I) The lysates of O cells were immunoprecipitated with anti-NS5B or anti-Chk2 antibody (DCS-273), followed by immunoblotting analysis using anti-HCV NS5B antibody. The result of Western blot analysis of 1/10 of the cellular lysates with anti-NS5B antibody is also shown. (J) 293FT cells were cotransfected with 4 μg of pCX4bsr/NS5B (1B-1) and 4 μg of pcDNA3-HA-Chk2wt. The cell lysates were immunoprecipitated with anti-HA antibody (3F10), followed by immunoblotting analysis using either anti-HA (HA-7) or anti-HCV NS5B antibody. IP, immunoprecipitation; WB, Western blotting; IgG, immunoglobulin G.

O cells were immunoprecipitated with anti-ATM antibody, and then immunoblotting analysis using either anti-ATM or anti-NS5B antibody was performed. The results revealed that endogenous ATM bound to endogenous NS5B (Fig. 6E). Furthermore, we confirmed that ATM bound to NS5B in immunoprecipitation analysis using lysates from 293FT cells, in which NS5B (1B-1 strain) and FLAG-tagged ATM were overexpressed (Fig. 6F). Similarly, we confirmed that FLAG-tagged ATM bound to NS5B derived from O cell lysates in immunoprecipitation analysis using lysates from 293FT cells in which FLAG-tagged ATM was overexpressed (Fig. 6G). Finally, to determine which HCV protein binds to Chk2, the 293FT cell lysates of overexpressed HA-Chk2 were mixed with the O cell lysates and were immunoprecipitated with anti-HA antibody, followed by Western blot analysis using anti-HCV NS5B, anti-HCV NS5A, anti-HCV core protein, or anti-HA antibody. Consistent with the immunofluorescence result that Chk2 partially colocalized with NS5B (Fig. 5C), we observed that HA-tagged Chk2 bound to NS5B (Fig. 6H). Importantly, we found that endogenous Chk2 bound to endogenous NS5B derived from O cells (Fig. 6I). In addition, HA-tagged Chk2 bound to NS5B in immunoprecipitation analysis using lysates from 293FT cells in which NS5B (1B-1 strain) and HA-tagged Chk2 were overexpressed (Fig. 6J). Thus, Chk2 also interacted with NS5B as well as ATM. Taking these results together, we conclude that HCV targets ATM and Chk2 DNA damage sensors and that the ATM signaling pathway is required for HCV RNA replication.

DISCUSSION

ATM has been implicated as a target of most DNA viruses, harboring their genomes in the form of dsDNA which can activate or inhibit the ATM signaling pathway (17). In this study, we have demonstrated for the first time that the ATM signaling pathway is required for HCV RNA replication even though HCV does not have a dsDNA genome, unlike DNA viruses. In this regard, Machida et al. previously proposed that HCV infection and the expression of HCV NS3 and core protein induced dsDNA breaks (18, 19). Furthermore, NS3 has DNA helicase activity by which it unwinds dsDNA, suggesting that NS3 affects host dsDNA (22, 25). Thus, HCV infection might trigger the activation of ATM without a dsDNA genome. In fact, we observed weak but significant phosphorylation of Chk2 at threonine 68, the specific marker for ATM activation, in the HCV RNA-replicating cells (O and sO cells) but not in the HCV-negative Oc and sOc cells (Fig. 3A), suggesting that the ATM-dependent DNA damage response is constantly stimulated in persistent HCV RNA-replicating cells. Furthermore, we demonstrated that ATM preferentially bound to NS3-4A over NS3 alone (Fig. 5B) and that ATM partially colocalized with NS3-4A in the perinuclear region, where HCV is known to form a replication complex and replicate itself, and in dispersed points throughout the cytoplasm (Fig. 5A), indicating the interaction of ATM with NS3-4A. Interestingly, Lai et al. very recently reported that NS3-4A impaired DNA repair and enhanced sensitivity to ionizing radiation through interaction with ATM (15). However, we observed an equivalent level of Chk2 phosphorylation at threonine 68, a direct downstream target of ATM (20, 21), in both HCV RNA-replicating cells (O cells) and HCV-negative cells (Oc cells) after treatment with adriamycin (Fig. 3A), suggesting that Chk2 phosphorylation by ATM is not impaired by HCV RNA replication. In this regard, Gaspar and Shenk also showed that human cytomegalovirus could inhibit a DNA damage response by mislocalizing ATM and phosphorylated Chk2 at threonine 68 to a cytoplasmic virus assembly zone, indicating that human cytomegalovirus blocked at the level of Chk2 (9). On the other hand, dsDNA triggers IFN immune defenses through retinoic acid-induced gene I, the mitochondrial antiviral signaling protein, or the DNA-dependent activator of IFN-regulatory factor (7, 26); and NS3-4A protease, which is known to cleave the mitochondrial antiviral signaling protein, can block it (26), suggesting that interaction of NS3-4A with ATM is partially involved in such a common antiviral signaling pathway. On the other hand, we previously demonstrated that HCV NS5B-expressing PH5CH8 immortalized human hepatocyte cells were susceptible to DNA damage in the form of dsDNA breaks (23). In this regard, we have found that HCV NS5B could bind to both ATM and Chk2 (Fig. 5B and C and 6E to J). Together, these results indicate that HCV might hijack ATM and Chk2 and utilize ATM and Chk2 for HCV RNA replication, thereby resulting in impairment of DNA repair, enhancement of mutation frequency, and development of hepatocellular carcinoma.

Finally, consistent with our finding that ATM was required for HCV RNA replication, an ATM kinase inhibitor efficiently suppressed genome-length HCV RNA replication at an EC_{50} of approximately 2 μM at 72 h after the treatment (Fig. 4A). Similarly, Lau et al. reported that the same ATM kinase inhibitor could suppress HIV-1 replication at an EC_{50} of approximately 2.3 μM (16). Importantly, the EC_{50} for HIV-1 replication is similar to that for HCV replication. Thus, this or other ATM kinase inhibitors may represent a novel approach for the clinical treatment of patients with chronic hepatitis C as well as AIDS patients.

ACKNOWLEDGMENTS

We thank D. Trono, R. Agami, R. Iggo, M. Kastan, S. J. Elledge, M. Kohara, A. Takamizawa, and M. Hijikata for the VSV-G-pseudotyped HIV-1-based vector system (pCMVR8.91 and pMDG2) and for pSUPER, pRDI292, pcDNA3-FLAG-ATM, and pcDNA3-HA-Chk2, and for anti-NS3 antibody, anti-NS5B antibody, anti-NS5A antibody, and 293FT cells. We also thank A. Morishita and T. Nakamura for their technical assistance.

This work was supported by a Grant-in-Aid for Young Scientists (B) from the Ministry of Education, Culture, Sports, Science and Technology (MEXT); by a Grant-in-Aid for Research on Hepatitis from the Ministry of Health, Labor, and Welfare of Japan; by the Ichiro Kanehara Foundation; and by a Research Fellowship from the Japan Society for the Promotion of Science.

REFERENCES

1. **Ariumi, Y., P. Turelli, M. Masutani, and D. Trono.** 2005. DNA damage sensors ATM, ATR, DNA-PKcs, and PARP-1 are dispensable for human immunodeficiency virus type 1 integration. J. Virol. **79:**2973–2978.
2. **Ariumi, Y., and D. Trono.** 2006. Ataxia-telangiectasia-mutated (ATM) protein can enhance human immunodeficiency virus type 1 replication by stimulating Rev. function. J. Virol. **80:**2445–2452.
3. **Ariumi, Y., M. Kuroki, K. Abe, H. Dansako, M. Ikeda, T. Wakita, and N. Kato.** 2007. DDX3 DEAD-box RNA helicase is required for hepatitis C virus RNA replication. J. Virol. **81:**13922–13926.
4. **Bridge, A. J., S. Pebernard, A. Ducraux, A.-L. Nicoulaz, and R. Iggo.** 2003. Induction of an interferon response by RNAi vectors in mammalian cells. Nat. Genet. **34:**263–264.

5. **Brummelkamp, T. R., R. Bernard, and R. Agami.** 2002. A system for stable expression of short interfering RNAs in mammalian cells. Science **296:**550–553.
6. **Canman, C. E., D.-S. Lim, K. A. Cimprich, Y. Taya, K. Tamai, K. Sakaguchi, E. Apella, M. B. Kastan, and J. D. Siliciano.** 1998. Activation of the ATM kinase by ionizing radiation and phosphorylation of p53. Science **281:**1677–1679.
7. **Cheng, G., J. Zhong, J. Chung, and F. V. Chisari.** 2007. Double-stranded DNA and double-stranded RNA induces a common antiviral signaling pathway in human cells. Proc. Natl. Acad. Sci. USA **104:**9035–9040.
8. **Dansako, H., M. Ikeda, and N. Kato.** 2007. Limited suppression of the interferon-beta production by hepatitis C virus serine protease in cultured human hepatocytes. FEBS J. **274:**4161–4176.
9. **Gaspar, M., and T. Shenk.** 2006. Human cytomegalovirus inhibits a DNA damage response by mislocalizing checkpoint proteins. Proc. Natl. Acad. Sci. USA **103:**2821–2826.
10. **Harper, J. W., and S. J. Elledge.** 2007. The DNA damage response: ten years after. Mol. Cell **28:**739–745.
11. **Ikeda, M., K. Abe, H. Dansako, T. Nakamura, K. Naka, and N. Kato.** 2005. Efficient replication of a full-length hepatitis C virus genome, strain O, in cell culture, and development of a luciferase reporter system. Biochem. Biophys. Res. Commun. **329:**1350–1359.
12. **Kato, N., M. Hijikata, Y. Ootsuyama, M. Nakagawa, S. Ohkoshi, T. Sugimura, and K. Shimotohno.** 1990. Molecular cloning of the human hepatitis C virus genome from Japanese patients with non-A, non-B hepatitis. Proc. Natl. Acad. Sci. USA **87:**9524–9528.
13. **Kato, N.** 2001. Molecular virology of hepatitis C virus. Acta Med. Okayama **55:**133–159.
14. **Kato, N., K. Sugiyama, K. Namba, H. Dansako, T. Nakamura, M. Takami, K. Naka, A. Nozaki, and K. Shimotohno.** 2003. Establishment of a hepatitis C virus subgenomic replicon derived from human hepatocytes infected in vitro. Biochem. Biophys. Res. Commun. **306:**756–766.
15. **Lai, C. K., K. S. Jeng, K. Machida, Y. S. Cheng, and M. M. Lai.** 2008. Hepatitis C virus NS3/4A protein interacts with ATM, impairs DNA repair and enhances sensitivity to ionizing radiation. Virology **370:**295–309.
16. **Lau, A., K. M. Swinbank, P. S. Ahmed, D. L. Taylor, S. P. Jackson, G. C. Smith, and M. J. O'Connor.** 2005. Suppression of HIV-1 infection by a small molecule inhibitor of the ATM kinase. Nat. Cell Biol. **7:**493–500.
17. **Lilley, C. E., R. A. Schwartz, and M. D. Weitzman.** 2007. Using or abusing: viruses and the cellular DNA damage response. Trends Microbiol. **15:**119–126.
18. **Machida, K., K. T. Cheng, V. M. Sung, S. Shimodaira, K. L. Lindsay, A. M. Levine, M. Y. Lai, and M. M. Lai.** 2004. Hepatitis C virus induces a mutator phenotype: enhanced mutations of immunoglobulin and protooncogenes. Proc. Natl. Acad. Sci. USA **101:**4262–4267.
19. **Machida, K., K. T. Cheng, V. M. Sung, K. J. Lee, A. M. Levine, and M. M. Lai.** 2004. Hepatitis C virus infection activates the immunologic (type II) isoform of nitric oxide synthase and thereby enhances DNA damage and mutations of cellular genes. J. Virol. **78:**8835–8843.
20. **Matsuoka, S., M. Huang, and S. J. Elledge.** 1998. Linkage of ATM to cell cycle regulation by the Chk2 protein kinase. Science **282:**1893–1897.
21. **Matsuoka, S., G. Rotman, A. Ogawa, Y. Shiloh, K. Tamai, and S. J. Elledge.** 2000. Ataxia telangiectasia-mutated phosphorylates Chk2 in vivo and in vitro. Proc. Natl. Acad. Sci. USA **97:**10389–10394.
22. **Myong, S., M. M. Bruno, A. M. Pyle, and T. Ha.** 2007. Spring-loaded mechanism of DNA unwinding by hepatitis C virus NS3 helicase. Science **317:**513–516.
23. **Naka, K., H. Dansako, N. Kobayashi, M. Ikeda, and N. Kato.** 2006. Hepatitis C virus NS5B delays cell cycle progression by inducing interferon-β via Toll-like receptor 3 signaling pathway without replicating viral genomes. Virology **346:**348–362.
24. **Naldini, L., U. Blömer, P. Gallay, D. Ory, R. Mulligan, F. H. Gage, I. M. Verma, and D. Trono.** 1996. In vivo gene delivery and stable transduction of nondividing cells by a lentiviral vector. Science **272:**263–267.
25. **Pang, P. S., E. Jankowsky, P. J. Planet, and A. M. Pyle.** 2002. The hepatitis C viral NS3 protein is a processive DNA helicase with cofactor enhanced RNA unwinding. EMBO J. **21:**1168–1176.
26. **Takaoka, A., Z. Wang, M. K. Choi, H. Yanai, H. Negishi, T. Ban, Y. Lu, M. Miyagishi, T. Kodama, K. Honda, Y. Ohba, and T. Taniguchi.** 2007. DAI (DLM-1/ZBP1) is a cytosolic DNA sensor and an activator of innate immune response. Nature **448:**501–505.
27. **Tanaka, T., N. Kato, M. J. Cho, and K. Shimotohno.** 1995. A novel sequence found at the 3′ terminus of hepatitis C virus genome. Biochem. Biophys. Res. Commun. **215:**744–749.
28. **Thomas, D. L.** 2000. Hepatitis C epidemiology. Curr. Top. Microbiol. Immunol. **242:**25–41.
29. **Wakita, T., T. Pietschmann, T. Kato, T. Date, M. Miyamoto, Z. Zhao, K. Murthy, A. Habermann, H. G. Kräusslich, M. Mizokami, R. Bartenschlager, and T. J. Liang.** 2005. Production of infectious hepatitis C virus in tissue culture from a cloned viral genome. Nat. Med. **11:**791–796.
30. **Zufferey, R., D. Nagy, R. J. Mandel, L. Naldini, and D. Trono.** 1997. Multiply attenuated lentiviral vector achieves efficient gene delivery in vivo. Nat. Biotechnol. **15:**871–875.

Biochemical and Biophysical Research Communications 371 (2008) 104–109

Contents lists available at ScienceDirect

Biochemical and Biophysical Research Communications

journal homepage: www.elsevier.com/locate/ybbrc

New efficient replication system with hepatitis C virus genome derived from a patient with acute hepatitis C ☆

Kyoko Mori, Ken-ichi Abe, Hiromichi Dansako, Yasuo Ariumi, Masanori Ikeda, Nobuyuki Kato *

Department of Molecular Biology, Okayama University Graduate School of Medicine, Dentistry, and Pharmaceutical Sciences, 2-5-1 Shikata-cho, Okayama 700-8558, Japan

ARTICLE INFO

Article history:
Received 25 March 2008
Available online 10 April 2008

Keywords:
Hepatitis C virus
Acute hepatitis C
HCV replication system
Genome-length HCV RNA
Anti-HCV reagents
Interferon-γ

ABSTRACT

We report for the first time a new RNA replication system with a hepatitis C virus (HCV) strain (AH1) derived from a patient with acute hepatitis C. Using an HCV replicon RNA library constructed with the AH1 strain (genotype 1b), we first established a cloned cell line, sAH1, harboring the HCV replicon. Cured cells obtained with interferon treatment of sAH1 cells were used for transfection with genome-length HCV RNA possessing four mutations found in sAH1 replicon. Consequently, one cloned cell line, AH1, supporting efficient replication of genome-length HCV RNA was obtained. By the comparison of AH1 cells with the O cells supporting genome-length HCV RNA (HCV-O strain) replication, we found different anti-HCV profiles of interferon-γ and cyclosporine A between AH1 and O cells. Reporter assay analysis suggests that the diverse effects of interferon-γ are due to the difference in HCV strains, but not the cellular environment.

Hepatitis C virus (HCV) infection frequently causes chronic hepatitis, which progresses to liver cirrhosis and hepatocellular carcinoma. HCV infection has now become a serious health problem because at least 170 million people worldwide are currently infected with HCV [1]. HCV is an enveloped virus with a positive single-stranded 9.6 kilobase (kb) RNA genome, which encodes a large polyprotein precursor of approximately 3000 amino acid (aa) residues [2,3]. This polyprotein is cleaved by a combination of the host and viral proteases into at least 10 proteins in the following order: core, envelope 1 (E1), E2, p7, non-structural 2 (NS2), NS3, NS4A, NS4B, NS5A, and NS5B [3].

As a striking breakthrough in HCV research, in 1999, an HCV replicon system enabling robust HCV subgenomic RNA (Con-1 strain of genotype 1b) replication in specific human HuH-7 hepatoma cells has been developed [4]. After the first Con-1 replicon, several HCV replicon (genotypes 1a, 1b, and 2a) systems using HuH-7-derived cells have been developed. These replicon systems have become powerful tools for basic studies of HCV replication, HCV–host cell interactions, and screening of anti-HCV reagents, [5,6]. Furthermore, genome-length HCV RNA replication systems have been developed [7–9], since HCV replicons lacking HCV structural proteins are insufficient for further HCV research. We also established a genome-length HCV RNA-replicating cell line (HCV-O strain of genotype 1b; called O cell line) [10] using cured cells derived from sO cells [11], in which HCV replicon RNA (HCV-O strain) with an adaptive mutation (S2200R) is replicating. However, to date, established genome-length HCV RNA-replicating stable cell lines are limited to five HCV strains, H77 (1a), HCV-N (1b), Con-1 (1b), HCV-O (1b), and JFH1 (2a) [7–10,12], and there is no RNA replication system with an HCV strain derived from a patient with acute hepatitis C. Furthermore, there have been few reports comparing these HCV strains.

To clarify these problems, we have attempted to establish a new stable cell line, in which genome-length HCV RNA derived from a patient with acute hepatitis C is efficiently replicating. We report herein a new efficient RNA replication system with HCV derived from a patient with acute hepatitis C and provide a comparative analysis of RNA replication systems with AH1 and HCV-O strains regarding the sensitivities to anti-HCV reagents, including interferon (IFN)-α.

Materials and methods

Cell culture. Cells supporting HCV replicon or genome-length HCV RNA, and cured cells, from which the HCV RNA had been eliminated by IFN treatment, were maintained as described previously [10].

Reverse transcription (RT)-nested PCR. RNA from a serum of patient AH1 [13] with acute hepatitis C was prepared using the ISOGEN-LS extraction kit (Nippon Gene Co., Japan). This RNA sample was used as a template for RT-nested PCR to amplify the HCV RNA. RT-nested PCR was performed separately in two parts; one part (3.5 kb) covered from HCV 5′UTR to NS3, and the other part (6 kb) covered from NS2 to NS5B. For the first part, the antisense primer AH3553R, 5′-CACACGCCGTTGATGC AGGTCG-3′ was used for RT. Primers 21 [11] and AH3519R, 5′-TGCGTGGCGG

☆ The nucleotide sequence data reported in this paper will appear in the DDBJ, EMBL, and GenBank nucleotide sequence databases under Accession No. AB429050.

* Corresponding author. Fax: +81 86 235 7392.
E-mail address: nkato@md.okayama-u.ac.jp (N. Kato).

0006-291X/$ - see front matter © 2008 Elsevier Inc. All rights reserved.
doi:10.1016/j.bbrc.2008.04.005

TGGAAACCACCTG-3' were employed in the first round of PCR (35 cycles). An internal primer pair (21X [11] and AH3466RX: 5'-ATTATTCTAGAGGCCTGTGAGACTG GTGATGATGC-3'; containing a XbaI site (underlined)) was used for the second round of PCR (35 cycles). For the second part, the antisense primer 386R [11] was used for RT. Primers 542 and 9388R [11] were employed in the first round of PCR (35 cycles). An internal primer pair (3295X: 5'-ATTATTCTAGACTGACATGGA GACCAAGATCATCAC-3'; containing a XbaI site (underlined) and 9357RX: 5'-ATTATT CTAGACCCGTTCACCGGTTGGGGAGCAG-3'; containing a XbaI site (underlined)) was used for the second round of PCR (35 cycles). These fragments overlapped at the NS2 and NS3 regions and were used for sequence analysis for HCV RNA after cloning into the XbaI site of pBR322MC [11]. Superscript II (Invitrogen) and KOD-plus DNA polymerase (Toyobo, Osaka, Japan) were used for RT and PCR, respectively.

Plasmid construction. PCR product (NS3 to NS5B of AH1 strain) with primers 542 and 9388R was further amplified with primers 3501S: 5'-ATTATACTAGTCTCACAGG CCGGGACAAGAACC-3'; containing a SpeI site (underlined) and 9162RB: 5'-ATTATC GTACGGCCCAGTTGAAGAGGTACTTGCC-3'; containing a BsiWI site (underlined). The amplified fragment was digested with SpeI and BsiWI, and ligated into the replicon cassette plasmid pNSS1RZ2RU [11], which was predigested with SpeI and BsiWI. Using this ligation reaction mixture, a replicon RNA library (AH1N/3-5B in Supplementary Fig. 1) was prepared by a previously described method [11]. To make the plasmid pAH1N/C-5B/PL, LS, $(VA)_2$ containing full-length HCV polyprotein of AH1 strain, pON/C-5B containing full-length HCV polyprotein of HCV-O strain [10] was utilized. First, to make a fragment for pAH1N/C-5B (Supplementary Fig. 1), overlapping PCR was used to fuse EMCV IRES to the core protein-coding sequence of the AH1 strain, as described previously [10]. The resulting DNA was digested with PmeI and ClaI, and then replaced with the PmeI–ClaI fragment of pON/C-5B (pON/C-5B/CoreAH was obtained). Second, the ClaI–AgeI fragment of pHCV-AH1 containing full-length HCV polyprotein of AH1 strain was replaced with the ClaI–AgeI fragment of pON/C-5B/CoreAH (pAH1N/C-5B was obtained). Finally, the SpeI–BsiWI fragment of pAH1N/3-5B clone 2 (see Fig. 1C) was replaced with the SpeI–BsiWI fragment of pAH1N/C-5B (pAH1N/C-5B/PL, LS, $(VA)_2$ was obtained).

RNA synthesis. Plasmid DNAs were linearized by XbaI and were used for RNA synthesis with T7 MEGAscript (Ambion) as previously described [11].

RNA transfection and selection of G418-resistant cells. The transfection of HCV replicon RNA or genome-length HCV RNA synthesized in vitro into HuH-7-derived cells was performed by electroporation, and the cells were selected in the presence of G418 (0.3 mg/ml; Promega) for 3 weeks as described previously [11].

Quantification of HCV RNA. The quantitative RT-PCR (RT-qPCR) analysis for HCV RNA was performed by LightCycler PCR as described previously [10]. Experiments were done in triplicate.

Integration analysis. Genomic DNA was extracted from the cultured cells using the DNeasy Blood & Tissue Kit (QIAGEN). The HCV 5'UTR and the IFN-β gene were detected according to a PCR method described previously [11].

Western blot analysis. The preparation of cell lysates, sodium dodecyl sulfate-polyacrylamide gel electrophoresis, and immunoblotting analysis were performed as previously described [11]. The antibodies used in this study were those against Core, E2, NS3, NS4A, NS5A, and NS5B [10]. β-Actin antibody (AC-15, Sigma) was used as the control for the amount of protein loaded per lane. Immunocomplexes were detected with the Renaissance enhanced chemiluminescence assay (Perkin-Elmer Life Sciences, Boston, MA).

Sequence analysis of HCV RNA. To amplify replicon RNA and genome-length HCV RNA, RT-PCR was performed as described previously [10,11]. The PCR products were subcloned into the XbaI site of pBR322MC, and sequence analysis was performed as described previously [11].

Northern blot analysis. Total RNA was extracted from the cultured cells using the RNeasy Mini Kit (QIAGEN). Three micrograms of total RNA was used for the analysis. HCV-specific RNA and β-actin were detected according to a method described previously [10].

Luciferase reporter assay. For the dual-luciferase assay, firefly luciferase vectors, pGBP-1(-216)-Luc and p2'-5'-OAS(-159)-Luc [14], were used. The reporter assay was performed as previously described [14]. The experiments were performed in at least triplicate.

Statistical analysis. Differences between AH1 and O cell lines were tested using the Student's *t*-test. *P* values <.05 were considered statistically significant.

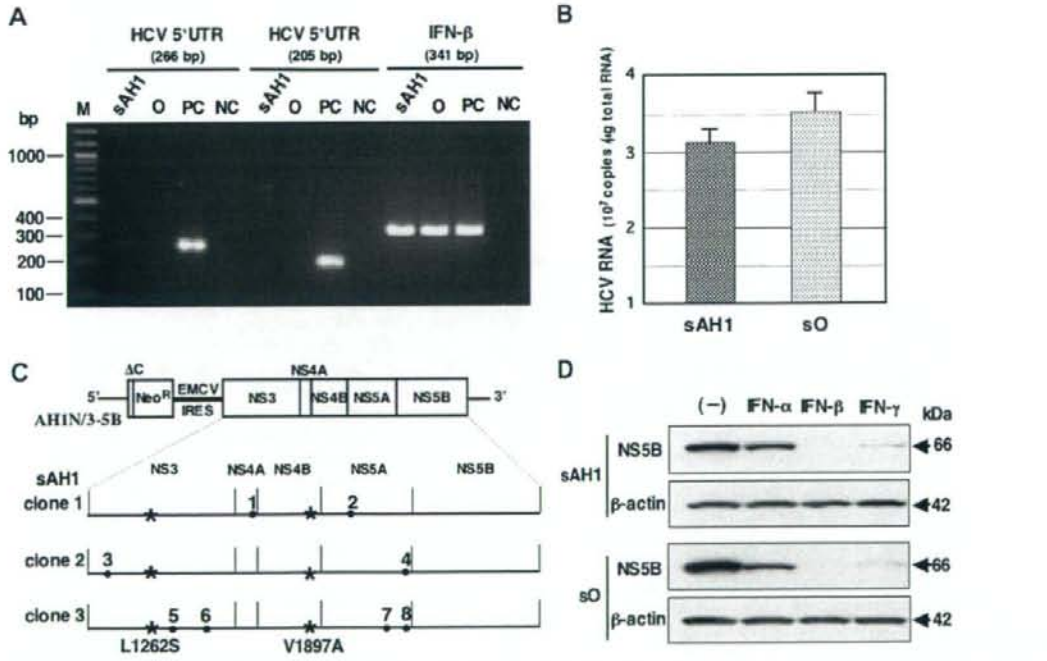

Fig. 1. Characterization of sAH1 cells harboring HCV replicon. (A) No integration of the HCV sequence in the genomic DNA. Genomic DNA from sAH1cells was subjected to PCR for the detection of the HCV 5'UTR and the IFN-β gene. O cells were used as a negative control. Lane PC, HCV sequence-integrated cells; lane NC, no genomic DNA; lane M, 100 bp DNA ladder. PCR products were detected by staining with ethidium bromide after 3% agarose gel electrophoresis. (B) Quantitative analysis of intracellular replicon RNA. The levels of replicon RNA were quantified by LightCycler PCR. sO cells harboring HCV-O replicon [11] were used for the comparison. (C) Amino acid substitutions detected in intracellular AH1 replicon RNA. NS3 to NS5B regions of three independent clones sequenced were presented. L1262S and V1897A conserved substitutions are indicated by asterisks. Clone-specific aa substitutions (indicated by the numbers with dots) are as follows: 1, K1691R; 2, M2105I; 3, P1115L; 4, V2360A; 5, K1368R; 6, A1533T; 7, I2285V; 8, D2377H. (D) IFN sensitivity of AH1 replicon. sAH1 cells were treated with IFN-α (Sigma), IFN-β (a gift from Toray Industries), and IFN-γ (Sigma) (20 IU/ml each) for 5 days. For the comparison, sO cells were treated as well as sAH1 cells. NS5B was detected by Western blot analysis.

Results

Establishment of a G418-resistant cell line (sAH1) harboring HCV replicon RNA

An HCV replicon RNA library prepared from the AH1 strain was first transfected into sOc cells (cured sO cells) [11], and the G418-resistant cells were selected as described previously [11]. Although several G418-resistant colonies were obtained, production of these colonies was due to integration of the HCV RNA sequence into the chromosomal DNA (PC in Fig. 1A). Therefore, we further cleaned up the replicon RNA library with additional DNase treatment, and it was then transfected into OR6c cells (cured OR6 cells) [10]. Consequently, a G418-resistant colony was obtained and successfully proliferated; this colony was referred to as sAH1. To exclude the possibility of integration of a replicon RNA sequence into the genomic DNA, we examined the presence of the HCV 5′UTR sequence in the genomic DNA isolated from sAH1 cells by a PCR method described previously [11]. Genome-length HCV RNA-replicating O cells were also examined as a negative control. The results revealed that the HCV RNA sequence was not integrated into the genomic DNA in either sAH1 cells or O cells (Fig. 1A).

Regarding the level of replicon RNA in sAH1 cells, RT-qPCR analysis revealed that the titer of replicon RNA was approximately 3×10^7 copies/μg total RNA, and its level was equivalent to that in sO cells (Fig. 1B), suggesting that the efficiency of RNA replication in sAH1 cells is similar to that in sO cells.

To exclude the possibility that sAH1 cells were derived from a small number of OR6 cells remaining after IFN treatment, and to determine whether replicon RNA in sAH1 cells possesses cell culture-adaptive mutations [5], which enhance the efficiency of RNA replication, we performed genetic analysis of the intracellular AH1 replicon. The sequences of three independent clones were determined and compared with each other to avoid PCR error. The obtained consensus nucleotide and aa sequences of NS3–NS5B regions of the AH1 replicon showed 7.3% and 3.7% differences, respectively, from those of the HCV-O replicon [11], indicating that sAH1 cells were not contaminated by the OR6 cells. In contrast, to find conserved mutations in the AH1 replicon, we determined the consensus nucleotide sequences of AH1 serum-derived HCV RNA by comparison of the nucleotide sequences of three independently isolated cDNA clones (Accession No. AB429050). The K1609E (NS3) and S2200R (NS5A) adaptive mutations found in O and OR6 cells were not detected in the AH1 replicon. However, instead of these mutations, L1262S (NS3) and V1897A (NS4B) conserved mutations were detected (Fig. 1C). Although V1897A has been detected as an adaptive mutation in Con-1 replicon [15], L1262S has until now remained undetected. In clone 2, the P1115L mutation (number 3 in Fig. 1C), which has been reported as an adaptive mutation [15,16], was detected.

To further characterize the sAH1 replicon, we compared the sensitivities of sAH1 and sO replicons against anti-HCV reagents (IFN-α, IFN-β, and IFN-γ) [5,6,11]. Western blot analysis of NS5B revealed that the IFN sensitivity of the sAH1 replicon was equivalent to that of the sO replicon (Fig. 1D).

Establishment of a genome-length HCV-AH1 RNA-replicating cell line, AH1

To develop a genome-length HCV RNA replication system, we first constructed a pAH1N/C-5B/PL, LS, $(VA)_2$ by the replacement with sAH1 replicon clone 2 (Fig. 1C) into pAH1N/C-5B. AH1N/C-5B/PL, LS, $(VA)_2$ RNA was transfected into sAH1c cells, cured sAH1 cells. Following 3 weeks of culturing in the presence of

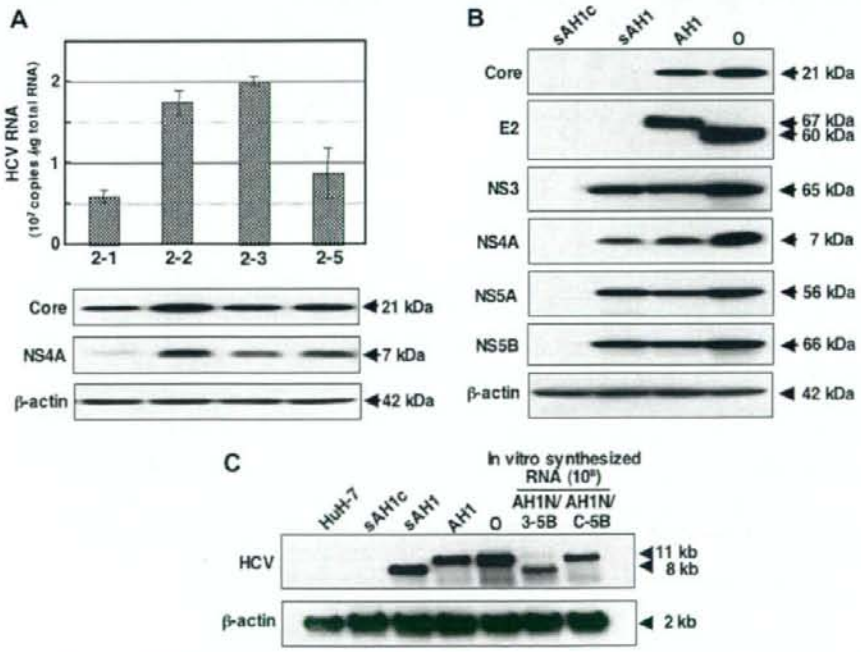

Fig. 2. Characterization of AH1 cells harboring genome-length HCV RNA. (A) Selection of G418-resistant cell lines. The levels of HCV RNA in G418-resistant cells were quantified by LightCycler PCR (upper panel). Core and NS4A were detected by Western blot analysis (lower panel). (B) Western blot analysis. AH1, O, sAH1, and sAH1c cells were used for the comparison. Core, E2, NS3, NS4A, NS5A, and NS5B were detected by Western blot analysis. (C) Northern blot analysis. AH1, O, sAH1, sAH1c, and HuH-7 cells were used for the comparison. In vitro-synthesized AH1N/3-5B and AH1N/C-5B RNAs were also used for the comparison.

G418, several colonies were obtained, and 4 colonies (2-1, 2-2, 2-3, and 2-5) then successfully proliferated. We selected colony 2-2 among them because it showed high levels of HCV RNA and proteins (core and NS4A) (Fig. 2A); this cell line was referred to as AH1. To compare the expression levels of HCV proteins in AH1 cells with those in O cells, Western blot analysis was further performed. Although the levels of HCV proteins in AH1 cells were slightly lower than those in O cells, the expression levels of NS proteins in AH1 cells were equivalent to those in sAH1 cells (Fig. 2B). In this analysis, we noticed that the size of the E2 protein in AH1 cells was 7 kDa larger than that in O cells (Fig. 2B). This difference may be due to the different numbers of *N*-glycosylation sites in E2 protein, since 11 and 9 *N*-glycosylation sites in E2 proteins are estimated in AH1 and HCV-O strains, respectively. Northern blot analysis also showed the presence of HCV-specific RNA with a length of approximately 11 kb in the extracts of total RNA prepared from AH1 cells, similar to that in the O cells (Fig. 2C). We confirmed the presence of replicon RNA (approximately 8 kb) in sAH1 cells (Fig. 2C). To check the additional adaptive mutations in the genome-length AH1 RNA, we performed sequence analysis of HCV RNA in AH1 cells. The results (Supplementary Fig. 2) revealed no additional mutations detected commonly among the three independent clones sequenced, suggesting that additional adaptive mutations are not required for genome-length HCV RNA replication. We therefore conclude that the AH1 cell line can be used as a genome-length HCV RNA replication system with acute hepatitis C-derived HCV strain.

Diverse effects of anti-HCV reagents on HCV RNA replication in AH1 and O cells

To compare the effects of anti-HCV reagents on RNA replication systems with different HCV strains, we examined the anti-HCV profiles of IFN-α, IFN-γ, and cyclosporine A (CsA) [17] using AH1 and O cells. Regarding IFN-α, the anti-HCV effect in AH1 cells was similar to that in O cells (Fig. 3A). Although RT-qPCR analysis showed a statistically significant difference in both cell systems when 1 IU/ml of IFN-α was used, such a difference was not observed in the Western blot analysis (Fig. 3A). In contrast, a significant different effect of IFN-γ was observed in both cell systems. RT-qPCR and Western blot analyses revealed that RNA replication of the AH1 strain was less sensitive than that of the HCV-O strain when 1 or 10 IU/ml of IFN-γ was used (Fig. 3B). Conversely, we observed that RNA replication of the AH1 strain was more sensitive to CsA than that of the HCV-O strain (Fig. 3C). These results suggest that anti-HCV profiles of IFN-γ and CsA are rather different between AH1 and O cell systems.

Different anti-HCV profile of IFN-γ is not correlated with the cellular potentials of the IFN-γ signaling pathway

To clarify whether the different effects of IFN-γ observed between AH1 and O cells are dependent on the cellular potentials of the IFN-γ signaling pathway, we performed a dual-luciferase reporter assay using an IFN-γ-inducible intrinsic GBP-1 gene promoter. As a control, IFN-α-inducible intrinsic 2′–5′-OAS gene promoter was also used for the analysis of the IFN-α signaling pathway. The results revealed that a good response of both AH1 and O cells to IFN-α and IFN-γ stimulation, with their potentials for both signaling pathways being almost the same (Fig. 4). These results suggest that the diverse anti-HCV effects of IFN-γ are dependent on the HCV strain, but not on the cellular potentials of the IFN-γ signaling pathway.

Discussion

In the present study, we established for the first time an HCV RNA replication system with AH1 strain derived from a patient

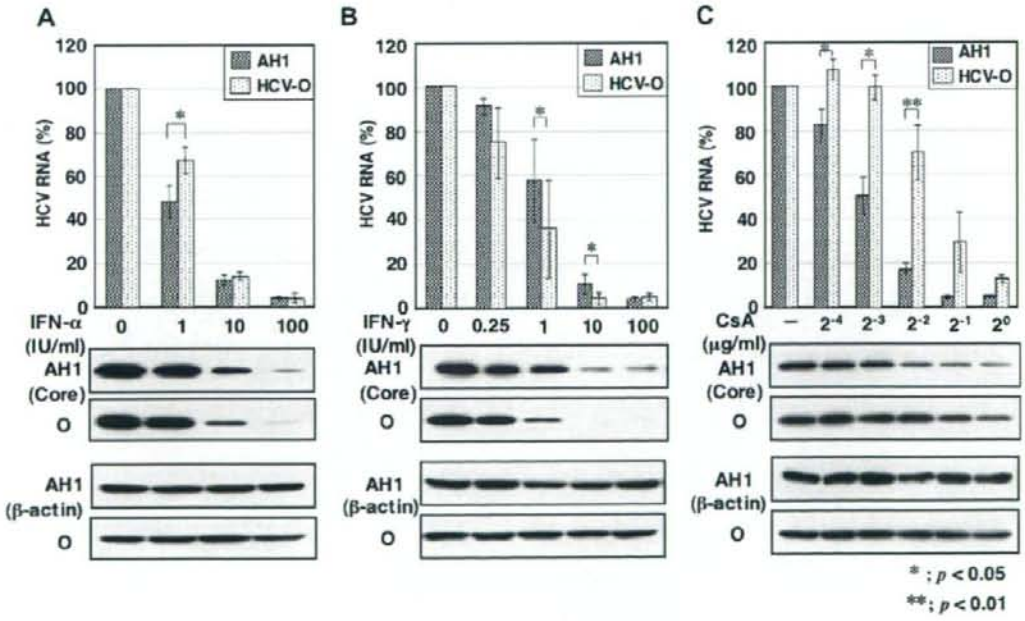

Fig. 3. The diverse effects of anti-HCV reagents on AH1 and HCV-O RNA replications. AH1 and O cells were treated with anti-HCV reagents for 72 h, and then extracted total RNAs and cell lysates were subjected to RT-qPCR for HCV 5′ UTR (each upper panel) and Western blot analysis for the core protein (each lower panel), respectively. (A) Effect of IFN-α. (B) Effect of IFN-γ. (C) Effect of CsA (Sigma).

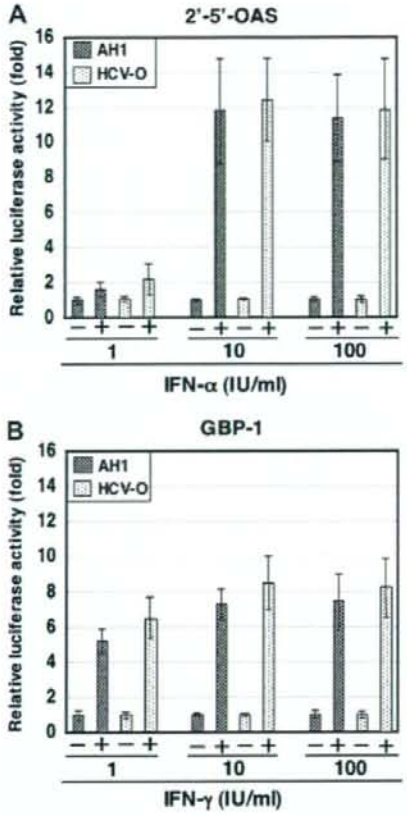

Fig. 4. Dual-luciferase reporter assay of IFN-α or IFN-γ-inducible gene promoter. AH1 and O cells were treated for 6 h with IFN-α or IFN-γ before the reporter assay. (A) 2′–5′-OAS gene promoter. (B) GBP-1 gene promoter.

with acute hepatitis C, and found diverse anti-HCV effects of IFN-γ and CsA between AH1 and HCV-O strains.

The levels of HCV replicon RNA and genome-length HCV RNA in sAH1 and AH1 cells were assigned to 3×10^7 and 2×10^7 copies/μg total RNA, respectively. These values are similar to those obtained from previously established HCV RNA replication systems [5]. Since known adaptive mutations (P1115L and V1897A) and additional conserved mutations (L1262S) were detected in the developed sAH1 replicon, these mutations may contribute to enhanced levels of RNA replication. The expression levels of genome-length HCV RNA and proteins observed in the present study suggest that genome-length HCV RNA replication efficiently occurs in AH1 cells, and that this RNA replication system is useful for comparison with already developed genome-length HCV RNA replication systems with HCV-N [7], Con-1 [8,9], or HCV-O [10] strains.

In the comparative analysis of genome-length HCV RNA replication systems with AH1 and HCV-O strains, we found that IFN-γ and CsA showed different anti-HCV profiles between AH1 and HCV-O strains. Regarding IFN-γ, RNA replication of the AH1 strain (EC_{50} = 1.9 IU/ml) was less sensitive than that of the HCV-O strain (EC_{50} = 0.3 IU/ml). Windisch et al. [18] have previously reported that RNA replication in an HCV replicon system using HuH-6 hepatoma cells is highly resistant (EC_{50} was more than 100 IU/ml) to IFN-γ, and that its resistant phenotype is not due to a general defect in the IFN-γ signaling pathway. In that study, they speculated that some mutations within a critical effector gene in HuH-6 cells might account for the inability of the cells to reduce the number of replicon RNAs in response to IFN-γ. Although such a possibility is not completely excluded, the diverse effects of IFN-γ observed in the present study were likely due to the difference in viral strains because RNA replication of the AH1 strain is still sensitive to IFN-γ. To clarify this point, development of an additional HCV RNA replication system such as an OR6 assay system with more quantitative reporter genes [10] is needed.

Regarding CsA, RNA replication of the AH1 strain (EC_{50} = 0.13 μg/ml) showed more sensitivity than that of the HCV-O strain (EC_{50} = 0.35 μg/ml). Ishii et al. [17] have previously reported that RNA replication of the JFH1 strain (genotype 2a) is less sensitive to CsA than genotype 1b strains, including the HCV-O strain. In that study, they concluded that the difference in sensitivity of JFH1 and genotype 1b strains to CsA could be attributed to characteristic differences in the HCV strains, not to the parent cell strain. In addition, sensitivity to CsA was almost the same among genotype 1b strains in that study. Therefore, we estimate that the AH1 strain is more sensitive to CsA than these genotype 1b strains examined to date. Further analysis will be necessary to clarify the mechanism underlying differences in sensitivity to CsA among genotype 1b strains.

In conclusion, an HCV RNA replication system with the AH1 strain would be useful for comparison with other strain-derived systems in various HCV studies, including analysis of the effects of anti-HCV reagents.

Acknowledgments

We thank T. Nakamura for technical assistance. We also thank A. Takamizawa and M. Kohara for the anti-NS3, NS4A, NS5A, and NS5B antibodies. This work was supported by grants-in-aid for a third-term comprehensive 10-year strategy for cancer control, and for research on hepatitis from the Ministry of Health, Labor, and Welfare of Japan.

Appendix A. Supplementary data

Supplementary data associated with this article can be found, in the online version, at doi:10.1016/j.bbrc.2008.04.005.

References

[1] D.L. Thomas, Hepatitis C epidemiology, Curr. Top. Microbiol. Immunol. 242 (2000) 25–41.
[2] N. Kato, M. Hijikata, Y. Ootsuyama, M. Nakagawa, S. Ohkoshi, T. Sugimurd, K. Sugimurd, Molecular cloning of the human hepatitis C virus genome from Japanese patients with non-A, non-B hepatitis, Proc. Natl. Acad. Sci. USA 87 (1990) 9524–9528.
[3] N. Kato, Molecular virology of hepatitis C virus, Acta Med. Okayama 55 (2001) 133–159.
[4] V. Lohmann, F. Korner, J. Koch, U. Herian, L. Theilmann, R. Bartenschlager, Replication of subgenomic hepatitis C virus RNAs in a hepatoma cell line, Science 285 (1999) 110–113.
[5] R. Bartenschlager, S. Sparacio, Hepatitis C virus molecular clones and their replication capacity in vivo and in cell culture, Virus Res. 127 (2007) 195–207.
[6] J.M. Pawlotsky, S. Chevaliez, J.G. McHutchison, The hepatitis C virus life cycle as a target for new antiviral therapies, Gastroenterology 132 (2007) 1979–1998.
[7] M. Ikeda, M. Yi, K. Li, S.M. Lemon, Selectable subgenomic and genome-length dicistronic RNAs derived from an infectious molecular clone of the HCV-N strain of hepatitis C virus replicate efficiently in cultured Huh7 cells, J. Virol. 76 (2002) 2997–3006.
[8] T. Pietschmann, V. Lohmann, A. Kaul, N. Krieger, G. Rinck, G. Rutter, D. Strand, R. Bartenschlager, Persistent and transient replication of full-length hepatitis C virus genomes in cell culture, J. Virol. 76 (2002) 4008–4021.
[9] K.J. Blight, J.A. McKeating, J. Marcotrigiano, C.M. Rice, Efficient replication of hepatitis C virus genotype 1a RNAs in cell culture, J. Virol. 77 (2003) 3181–3190.

[10] M. Ikeda, K. Abe, H. Dansako, T. Nakamura, K. Naka, N. Kato, Efficient replication of a full-length hepatitis C virus genome, strain O, in cell culture, and development of a luciferase reporter system, Biochem. Biophys. Res. Commun. 329 (2005) 1350–1359.
[11] N. Kato, K. Sugiyama, K. Namba, H. Dansako, T. Nakamura, M. Takami, K. Naka, A. Nozaki, K. Shimotohno, Establishment of a hepatitis C virus subgenomic replicon derived from human hepatocytes infected in vitro, Biochem. Biophys. Res. Commun. 306 (2003) 756–766.
[12] T. Wakita, T. Pietschmann, T. Kato, T. Date, M. Miyamoto, Z. Zhao, K. Murthy, A. Habermann, H.G. Krausslich, M. Mizokami, R. Bartenschlager, T.J. Liang, Production of infectious hepatitis C virus in tissue culture from a cloned viral genome, Nat. Med. 11 (2005) 791–796.
[13] N. Kato, H. Sekiya, Y. Ootsuyama, T. Nakazawa, M. Hijikata, S. Ohkoshi, K. Shimotohno, Humoral immune response to hypervariable region 1 of the putative envelope glycoprotein (gp70) of hepatitis C virus, J. Virol. 67 (1993) 3923–3930.
[14] H. Dansako, A. Naganuma, T. Nakamura, F. Ikeda, A. Nozaki, N. Kato, Differential activation of interferon-inducible genes by hepatitis C virus core protein mediated by the interferon stimulated response element, Virus Res. 97 (2003) 17–30.
[15] V. Lohmann, S. Hoffmann, U. Herian, F. Penin, R. Bartenschlager, Viral and cellular determinants of hepatitis C virus RNA replication in cell culture, J. Virol. 77 (2003) 3007–3019.
[16] K. Abe, M. Ikeda, H. Dansako, K. Naka, N. Kato, Cell culture-adaptive NS3 mutations required for the robust replication of genome-length hepatitis C virus RNA, Virus Res. 125 (2007) 88–97.
[17] N. Ishii, K. Watashi, T. Hishiki, K. Goto, D. Inoue, M. Hijikata, T. Wakita, N. Kato, K. Shimotohno, Diverse effects of cyclosporine on hepatitis C virus strain replication, J. Virol. 80 (2006) 4510–4520.
[18] MP. Windisch, M. Frese, A. Kaul, M. Trippler, V. Lohmann, R. Bartenschlager, Dissecting the interferon-induced inhibition of hepatitis C virus replication by using a novel host cell line, J. Virol. 79 (2005) 13778–13793.

PPARα activation is essential for HCV core protein–induced hepatic steatosis and hepatocellular carcinoma in mice

Naoki Tanaka,[1,2] Kyoji Moriya,[3] Kendo Kiyosawa,[2] Kazuhiko Koike,[3] Frank J. Gonzalez,[4] and Toshifumi Aoyama[1]

[1]Department of Metabolic Regulation, Institute on Aging and Adaptation, Shinshu University Graduate School of Medicine, Matsumoto, Nagano, Japan.
[2]Division of Gastroenterology, Department of Internal Medicine, Shinshu University School of Medicine, Matsumoto, Nagano, Japan.
[3]Department of Infectious Diseases, Internal Medicine, Graduate School of Medicine, University of Tokyo, Tokyo, Japan.
[4]Laboratory of Metabolism, National Cancer Institute, NIH, Bethesda, Maryland, USA.

Transgenic mice expressing HCV core protein develop hepatic steatosis and hepatocellular carcinoma (HCC), but the mechanism underlying this process remains unclear. Because PPARα is a central regulator of triglyceride homeostasis and mediates hepatocarcinogenesis in rodents, we determined whether PPARα contributes to HCV core protein–induced diseases. We generated PPARα-homozygous, -heterozygous, and -null mice with liver-specific transgenic expression of the core protein gene (*Ppara*$^{+/+}$:HCVcpTg, *Ppara*$^{+/-}$:HCVcpTg, and *Ppara*$^{-/-}$:HCVcpTg mice. Severe steatosis was unexpectedly observed only in *Ppara*$^{+/+}$:HCVcpTg mice, which resulted from enhanced fatty acid uptake and decreased mitochondrial β-oxidation due to breakdown of mitochondrial outer membranes. Interestingly, HCC developed in approximately 35% of 24-month-old *Ppara*$^{+/+}$:HCVcpTg mice, but tumors were not observed in the other genotypes. These phenomena were found to be closely associated with sustained PPARα activation. In *Ppara*$^{+/-}$:HCVcpTg mice, PPARα activation and the related changes did not occur despite the presence of a functional *Ppara* allele. However, long-term treatment of these mice with clofibrate, a PPARα activator, induced HCC with mitochondrial abnormalities and hepatic steatosis. Thus, our results indicate that persistent activation of PPARα is essential for the pathogenesis of hepatic steatosis and HCC induced by HCV infection.

Introduction

HCV is one of the major causes of chronic hepatitis, whereas patients with persistent HCV infection have a high incidence of hepatocellular carcinoma (HCC) (1, 2). Occurrence of HCC associated with chronic HCV infection has increased over the past 2 decades (3–5), and chronic HCV infection is recognized as a serious debilitating disease. However, the mechanism in which chronic HCV infection mediates hepatocarcinogenesis remains unclear.

HCV core protein was shown to have oncogenic potential (6). To examine how HCV core protein participates in HCV-related hepatocarcinogenesis, transgenic mouse lines were established in which HCV core protein is expressed constitutively in liver at cellular levels similar to those found in chronic HCV-infected patients (7). These mice exhibited hepatic steatosis (7) and insulin resistance (8) as early as 3 months of age; on further aging, these symptoms worsened and hepatic adenomas developed in approximately 30% of mice between 16 and 18 months of age (9). Finally, HCC was found within hepatic adenomas in a classic "nodule-in-nodule" pathology (9). Interestingly, no hepatic inflammation or fibrosis was found in these mice throughout the course of HCC development (9), which suggested that the HCV core protein itself induces hepatic steatosis and HCC independently of hepatitis.

Several studies support the contention that hepatic steatosis promotes the development of HCC (10). Epidemiologic data have identified hepatic steatosis as a major accelerating factor of hepatocarcinogenesis in chronic HCV-infected patients (11). Moreover, increases in ROS production that can cause oxidative DNA damage, mitochondrial abnormalities, and accelerated hepatocyte proliferation were observed in the steatotic livers (12–14). Thus, an intriguing possibility has emerged that alteration of fatty acid metabolism in hepatocytes may be central to the pathogenesis of HCC induced by HCV core protein.

PPARs are ligand-activated nuclear receptors belonging to the steroid/thyroid hormone receptor superfamily; 3 isoforms designated as α, β/δ, and γ exist, all of which are involved in lipid homeostasis (15). PPARα regulates constitutive transcription of genes encoding fatty acid–metabolizing enzymes (16) and is associated with the maintenance of fatty acid transport and metabolism, primarily in liver, kidney, and heart. Administration of PPARα agonists, such as the widely prescribed fibrate drugs clofibrate, gemfibrozil, and fenofibrate, ameliorate hyperlipidemia in humans (17) and hepatic steatosis in mice (18).

On the other hand, long-term administration of PPARα ligands to rodents causes accelerated hepatocyte proliferation, increased ROS generation, and development of HCC (19, 20). Disruption of the PPARα gene was shown to prevent the development of HCC caused by long-term exposure to PPARα activators (21). Interestingly, accumulation of fatty acids/triglycerides in hepatocytes

Nonstandard abbreviations used: ACC, acetyl-CoA carboxylase; AOX, acyl-CoA oxidase; CDK, cyclin-dependent kinase; CYP4A1, cytochrome P450 4A1; FAS, fatty acid synthase; FAT, fatty acid translocase; FATP, fatty acid transport protein; HCC, hepatocellular carcinoma; HCVcpTg, HCV core protein–expressing transgenic; L-FABP, liver fatty acid-binding protein; MCAD, medium-chain acyl-CoA dehydrogenase; MTP, microsomal transfer protein; 8-OHdG, 8-hydroxy-2′-deoxyguanosine; PCNA, proliferating cell nuclear antigen; RXRα, retinoid X receptor α.

Conflict of interest: The authors have declared that no conflict of interest exists.

Citation for this article: *J. Clin. Invest.* **118**:683–694 (2008). doi:10.1172/JCI33594.

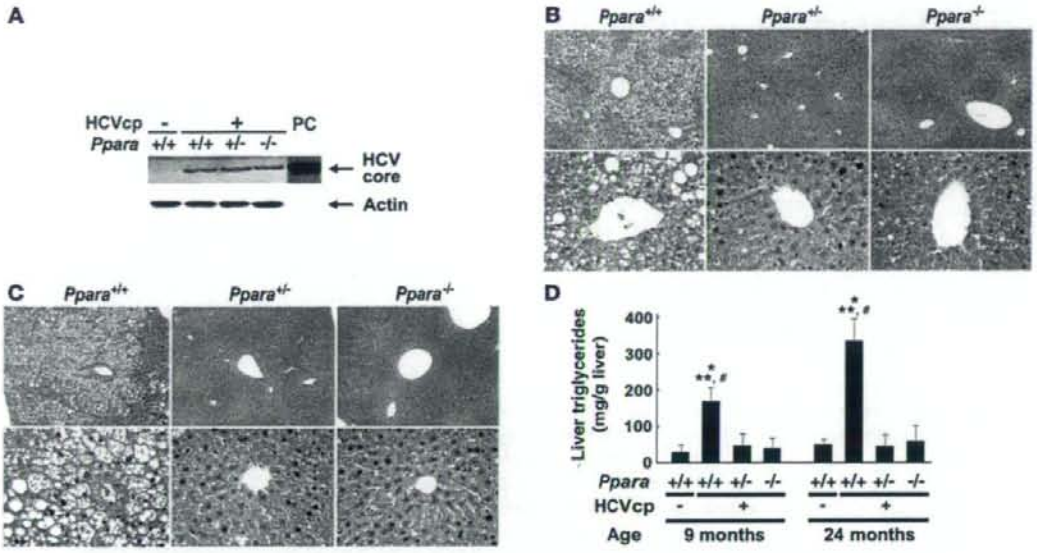

Figure 1

Phenotype changes in transgenic mouse liver. (**A**) Immunoblot analysis of HCV core protein expression in livers of 9-month-old mice. Because no significant individual differences in the same mouse group were found in the preliminary experiments, 10 mg of liver prepared from each mouse ($n = 6$ /group) was mixed and homogenized. Whole-liver lysate (50 μg protein) was loaded in each well. The band of actin was used as the loading control. Results are representative of 4 independent experiments. PC, lysate prepared from COS-1 cells overexpressing HCV core protein as a positive control. (**B**) Histological appearance of hematoxylin- and eosin-stained liver sections from 9-month-old HCVcpTg mice. Upper and lower rows show a lower (×40) and higher (×400) magnification, respectively. Microvesicular and macrovesicular steatosis was found only in *Ppara*$^{+/+}$:HCVcpTg mice. No inflammation or hepatocyte degeneration was evident in any of the genotypes. (**C**) Histological appearance of hematoxylin- and eosin-stained liver sections from 24-month-old HCVcpTg mice. Upper and lower rows show a lower (×40) and higher (×400) magnification, respectively. Hepatic steatosis was marked in *Ppara*$^{+/+}$:HCVcpTg mice, but not in other mice. Hepatic inflammation, fibrosis, and hepatocyte degeneration were not observed. In *Ppara*$^{+/-}$:HCVcpTg and *Ppara*$^{-/-}$:HCVcpTg mice, dysplastic hepatocytes and precancerous lesions were not detected throughout the entire liver. (**D**) Content of liver triglycerides. Results are expressed as the mean ± SD ($n = 6$/group) and compared between genotypes at the same age. $^{*}P < 0.05$ compared with *Ppara*$^{+/+}$ nontransgenic mice; $^{**}P < 0.05$ compared with *Ppara*$^{+/-}$:HCVcpTg mice; $^{\#}P < 0.05$ compared with *Ppara*$^{-/-}$:HCVcpTg mice.

could lead to continuous PPARα activation because of the presence of fatty acid metabolites that serve as natural PPARα ligands. For example, mice lacking expression of the peroxisomal acyl-CoA oxidase (AOX) gene showed massive accumulation of very-long-chain fatty acids in hepatocytes, severe microvesicular steatosis, chronic PPARα activation, and development of hepatic adenoma and HCC by 15 months of age (22). These results suggest a strong contribution of activated PPARα to liver tumorigenesis.

On the basis of several lines of evidence, we hypothesized that PPARα might contribute to hepatocarcinogenesis in HCV core protein–expressing transgenic (HCVcpTg) mice. To explore this possibility, PPARα-homozygous (*Ppara*$^{+/+}$), PPARα-heterozygous (*Ppara*$^{+/-}$), and PPARα-null (*Ppara*$^{-/-}$) mice bearing the HCV core protein gene, designated *Ppara*$^{+/+}$:HCVcpTg, *Ppara*$^{+/-}$:HCVcpTg, and *Ppara*$^{-/-}$:HCVcpTg mice, were generated, and phenotypic changes were examined. Surprisingly, we found that severe hepatic steatosis and HCC induced by HCV core protein developed only in *Ppara*$^{+/+}$ mice, which were related to persistent PPARα activation.

Results

Expression of HCV core protein in transgenic mice. *Ppara*$^{-/-}$:HCVcpTg and *Ppara*$^{+/-}$:HCVcpTg mice appeared healthy, and body weight in both genotypes was similar to that of *Ppara*$^{+/+}$:HCVcpTg and *Ppara*$^{+/+}$ mice without the transgene. When hepatic expression of HCV core protein in 9-month-old transgenic mice was examined by immunoblot analysis, it was similar among *Ppara*$^{+/+}$:HCVcpTg, *Ppara*$^{+/-}$:HCVcpTg, and *Ppara*$^{-/-}$:HCVcpTg mice (Figure 1A) and was also similar to expression in HCVcpTg mice reported previously (7, 9). Age and sex had only a minor influence on the hepatic expression of HCV core protein.

Requirement of homozygous PPARα for the development of hepatic steatosis in transgenic mice. Livers of 9-month-old male HCVcpTg mice with or without the *Ppara* allele were examined. Those of *Ppara*$^{+/+}$:HCVcpTg mice were soft, slightly enlarged, and light in color and histologically showed macrovesicular and microvesicular steatosis with no apparent inflammation or hepatocyte necrosis (Figure 1B), in agreement with previous reports (7, 9). Biochemical analysis of liver extracts showed marked hepatic accumulation of triglycerides (Figure 1D). In contrast, livers of 9-month-old *Ppara*$^{+/-}$:HCVcpTg and *Ppara*$^{-/-}$:HCVcpTg mice showed neither histological abnormalities nor accumulation of triglycerides (Figure 1, B and D). Hepatic levels of free fatty acids in *Ppara*$^{+/+}$:HCVcpTg mice were approximately 3 times those in *Ppara*$^{+/-}$:HCVcpTg and *Ppara*$^{-/-}$:HCVcpTg mice or *Ppara*$^{+/+}$ mice not expressing the HCV core protein.

In 24-month-old *Ppara*$^{+/+}$:HCVcpTg mice, hepatic steatosis was found (Figure 1C), and the hepatic levels of triglycerides were further increased (Figure 1D). Apparent inflammation, hepatocyte

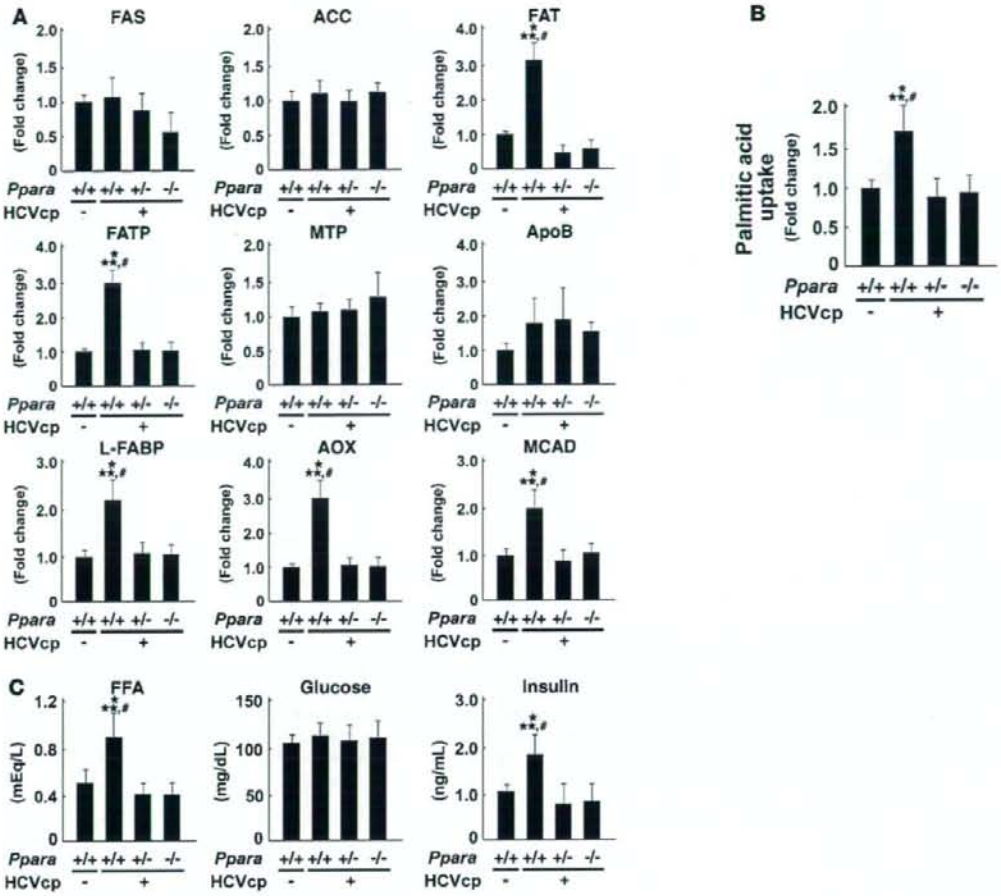

Figure 2

Analyses of factors associated with hepatic fatty acid and triglyceride metabolism. (**A**) Expression of genes associated with fatty acid and triglyceride metabolism in 9-month-old mouse livers. Total RNA was extracted from each mouse liver, and mRNA levels were determined by RT-PCR. mRNA levels were normalized by those of GAPDH and subsequently normalized by those in *Ppara*$^{+/+}$ nontransgenic mice. Results are expressed as the mean ± SD (n = 6/group). *P < 0.05 compared with *Ppara*$^{+/+}$ nontransgenic mice; **P < 0.05 compared with *Ppara*$^{+/-}$:HCVcpTg mice; #P < 0.05 compared with *Ppara*$^{-/-}$:HCVcpTg mice. (**B**) Uptake of fatty acids in 9-month-old mouse livers. Liver slices obtained from 3 mice in each group were incubated in medium containing 0.8 mM [1-^{14}C]palmitic acid for 7 h. Fatty acid uptake ability was estimated by the sum of palmitic acid converted to CO_2 and ketone bodies with that incorporated into total cellular lipids after incubation. The experiment was repeated 3 times. Results were normalized by those of *Ppara*$^{+/+}$ nontransgenic mice and expressed as the mean ± SD. (**C**) Plasma concentrations of free fatty acids, glucose, and insulin. After an overnight fast, blood was obtained from each mouse and the above variables were determined. Results are expressed as the mean ± SD (n = 6/group).

degeneration and necrosis, and fibrosis were not detected. On the other hand, *Ppara*$^{+/-}$:HCVcpTg and *Ppara*$^{-/-}$:HCVcpTg mice showed no steatosis (Figure 1, C and D). These results indicate that hepatic steatosis develops in *Ppara*$^{+/+}$:HCVcpTg mice, but not in *Ppara*$^{+/-}$:HCVcpTg and *Ppara*$^{-/-}$:HCVcpTg mice.

Hepatic fatty acid and triglyceride metabolism in transgenic mice. To investigate the mechanism responsible for the development of severe steatosis in *Ppara*$^{+/+}$:HCVcpTg mice, the expression of genes associated with fatty acid and triglyceride metabolism in the livers of 9-month-old mice was analyzed using the quantitative RT-PCR method. As shown in Figure 2A, the mRNA levels of genes related to de novo lipogenesis (fatty acid synthase [FAS] and acetyl-CoA carboxylase [ACC]) and secretion of VLDL (microsomal transfer protein [MTP] and apoB) were constant in all groups. The mRNA levels of fatty acid translocase (FAT) and fatty acid transport protein (FATP), which are associated with the uptake of fatty acids into hepatocytes, were significantly increased only in *Ppara*$^{+/+}$:HCVcpTg mice, but the mRNA levels of hepatic triglyceride lipase, another contributor to fatty acid uptake, remained unchanged (data not shown). The mRNA levels of liver fatty acid binding protein (L-FABP) were also elevated only in *Ppara*$^{+/+}$:HCVcpTg mice. Surprisingly, the mRNA levels of AOX and medium-chain acyl-CoA

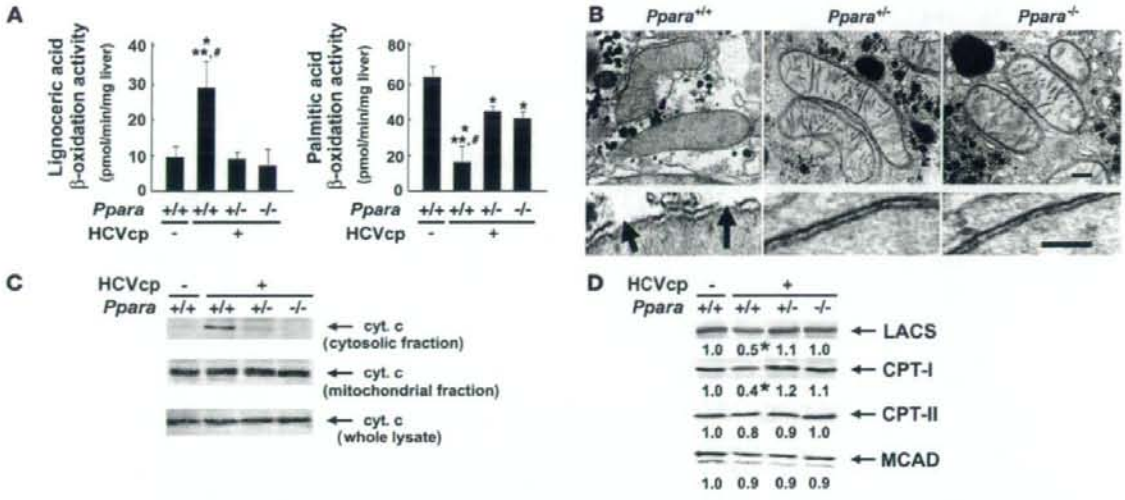

Figure 3

Analyses of mitochondrial abnormalities. (**A**) Lignoceric and palmitic acid β-oxidation activities in 9-month-old mice. Results are expressed as the mean ± SD (n = 6/group). *P < 0.05 compared with *Ppara*$^{+/+}$ nontransgenic mice; **P < 0.05 compared with *Ppara*$^{+/-}$:HCVcpTg mice; $^{\#}P$ < 0.05 compared with *Ppara*$^{-/-}$:HCVcpTg mice. (**B**) Electron microscopic features of hepatic mitochondria of 9-month-old HCVcpTg mice. Upper and lower rows show a lower and higher magnification, respectively. In *Ppara*$^{+/+}$:HCVcpTg mice, some mitochondria showing discontinuance of outer membranes (arrows) and amorphous inner structures were observed. In *Ppara*$^{+/-}$:HCVcpTg and *Ppara*$^{-/-}$:HCVcpTg mice, mitochondria appeared normal; the scale bars represent 200 nm (top) and 30 nm (bottom), respectively. (**C**) Immunoblot analysis of cytochrome *c* in 9-month-old mice. Whole-liver lysate, mitochondrial fraction, or cytosolic fraction (50 μg protein) was loaded in each well. Results are representative of 4 independent experiments. (**D**) Immunoblot analysis of representative mitochondrial β-oxidation enzymes using a mitochondrial fraction prepared from 9-month-old mouse livers. The mitochondrial fraction (20 μg protein) was loaded in each well. Results are representative of 4 independent experiments. The band intensity was quantified densitometrically and normalized by that in *Ppara*$^{+/+}$ nontransgenic mouse. The mean value of the fold changes is shown under the representative band. LACS, long-chain acyl-CoA synthase; CPT, carnitine palmitoyl-CoA transferase.

dehydrogenase (MCAD), a rate-limiting enzymes in the peroxisomal and mitochondrial β-oxidation pathways, respectively, were significantly increased in *Ppara*$^{+/+}$:HCVcpTg mice. When fatty acid uptake ability was measured in fresh liver slices, it was significantly enhanced only in *Ppara*$^{+/+}$:HCVcpTg mice (Figure 2B). Additionally, plasma free fatty acid levels were higher in these mice than in mice in the other groups. Although there were no differences in fasting plasma glucose levels between the groups, hyperinsulinemia was observed only in *Ppara*$^{+/+}$:HCVcpTg mice (Figure 2C), in agreement with the previous observation that significant insulin resistance developed in these mice (8). Similar results were obtained from 24-month-old mice (data not shown). These results combined show that the increased plasma fatty acid levels, which were likely due to enhanced peripheral fatty acid release caused by insulin resistance, and the increase in fatty acid uptake ability are consistent with steatogenesis in *Ppara*$^{+/+}$:HCVcpTg mice.

Decreased mitochondrial β-oxidation in transgenic mice. Although the transcriptional activities of major β-oxidation enzymes were markedly increased, *Ppara*$^{+/+}$:HCVcpTg mice had severe steatosis. To explore this discrepant result, peroxisomal and mitochondrial β-oxidation activities were measured using lignoceric and palmitic acids as substrates, respectively. The lignoceric acid–degrading capacity was increased only in *Ppara*$^{+/+}$:HCVcpTg mice, where it corresponded to an increase in AOX expression. However, the capacity for palmitic acid degradation, which occurs particularly in mitochondria, was significantly lower in *Ppara*$^{+/+}$:HCVcpTg mice than in *Ppara*$^{+/-}$:HCVcpTg and *Ppara*$^{-/-}$:HCVcpTg mice (Figure 3A). Thus, decreased mitochondrial β-oxidation ability was considered to be another important mechanism for the development of steatosis induced by the core protein.

We further evaluated mitochondrial abnormalities. In electron microscopic examination, discontinuous outer membranes (Figure 3B, arrows) and lack of an internal structure were observed in some mitochondria of *Ppara*$^{+/+}$:HCVcpTg mouse livers, in agreement with the previous report (9). However, these abnormalities were not seen in *Ppara*$^{+/-}$:HCVcpTg and *Ppara*$^{-/-}$:HCVcpTg mice (Figure 3B). Immunoblot analysis showed that cytochrome *c*, which is usually localized in the mitochondrial intermembrane space, was present in the cytosolic fractions of *Ppara*$^{+/+}$:HCVcpTg mice (Figure 3C). Moreover, immunoblot analysis using mitochondrial fractions showed that the expression levels of long-chain acyl-CoA synthase and carnitine palmitoyl-CoA transferase-I, which are enzymes indispensable to the initial step of mitochondrial β-oxidation and are localized mainly in mitochondrial outer membranes, were significantly decreased only in *Ppara*$^{+/+}$:HCVcpTg mice (Figure 3D).

Overall, these results suggest that homozygous PPARα is essential to the pathogenesis of hepatic steatosis induced by the HCV core protein, which results from a decrease in mitochondrial fatty acid degradation capacity caused by the breakdown of mitochondrial outer membranes and a disproportionate increase in the uptake of fatty acids. Interestingly, steatosis and the related changes did not occur in *Ppara*$^{+/-}$ and *Ppara*$^{-/-}$ mice expressing the HCV core protein, which suggested that these changes were not caused by the core protein itself.

Table 1
Incidence of HCC in 24-month-old mice

HCV core protein	*Ppara*	Mice (*n*)	Mice with HCC (*n*)	Incidence (%)
–	+/+	20	0	0
–	+/–	18	0	0
–	–/–	20	0	0
+	+/+	17	6	35.3[A]
+	+/–	16	0	0
+	–/–	14	0	0

Mice were killed at 24 months of age for analysis. HCC was diagnosed according to histological findings. [A]$P < 0.05$ compared with *Ppara*$^{+/+}$ nontransgenic mice, $P < 0.05$ compared with *Ppara*$^{+/-}$:HCVcpTg mice, $P < 0.05$ compared with *Ppara*$^{-/-}$:HCVcpTg mice.

Requirement of homozygous PPARα for hepatic tumor development in transgenic mice. At 9 months of age, hepatic nodules were not observed at all in transgenic mice, whereas, at 24 months, approximately 35% of *Ppara*$^{+/+}$:HCVcpTg mice had macroscopically evident hepatic nodules (Table 1). Microscopically, these nodules had the appearance of well-differentiated HCC with trabecular features, which was consistent with the previous report (9). Surprisingly, *Ppara*$^{+/-}$:HCVcpTg and *Ppara*$^{-/-}$:HCVcpTg mice of the same ages developed no evidence of hepatic tumors, despite the expression of HCV core protein at similar levels to those found in *Ppara*$^{+/+}$:HCVcpTg mice (Table 1). Microscopic examination showed that there were no dysplastic cells or precancerous lesions throughout the livers in *Ppara*$^{+/-}$:HCVcpTg and *Ppara*$^{-/-}$:HCVcpTg mice (Figure 1C). These results provide strong evidence that homozygous PPARα is essential for hepatic tumorigenesis induced by HCV core protein.

Increased hepatocyte proliferation only in Ppara$^{+/+}$*:HCVcpTg mice.* Because sustained acceleration of hepatocyte proliferation relative to apoptosis may promote the development of HCC, these opposing processes were quantified in the livers of 24-month-old mice. Both the liver-to-body weight ratio and the number of hepatocytes expressing proliferating cell nuclear antigen (PCNA) were increased only in *Ppara*$^{+/+}$:HCVcpTg mice (Figure 4, A and B). In contrast, the number of TUNEL-positive hepatocytes and the hepatic caspase 3 activity, indicators of hepatocyte apoptosis, remained similar among the 3 mouse strains (Figure 4, C and D). Interestingly, despite the presence of HCV core protein, the amounts of these proliferative and apoptotic markers in *Ppara*$^{+/-}$:HCVcpTg and *Ppara*$^{-/-}$:HCVcpTg mice were similar to those in *Ppara*$^{+/+}$ nontransgenic mice. Expression levels of several proteins, such as protooncogenes (c-Fos and c-Myc), cell-cycle regulators (cyclin D1, cyclin-dependent kinase [CDK] 4, and PCNA), and phosphorylated ERK 1 and 2, all of which are associated with hepatocyte proliferation, were elevated in *Ppara*$^{+/+}$:HCVcpTg mice but not in other genotypes (Figure 4, E and F).

Increased oxidative stress and DNA damage only in Ppara$^{+/+}$*:HCVcpTg mice.* HCV core protein is associated with increased production of ROS (23). Enhanced ROS production induces nuclear DNA damage, which results in the initiation of hepatocarcinogenesis, and can also injure organelles, which can result in disorders in their

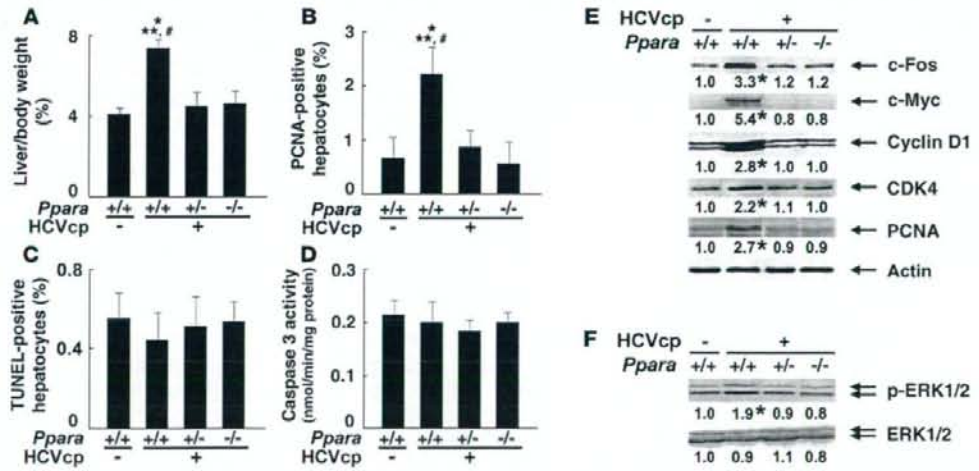

Figure 4
Increased hepatocyte proliferation in *Ppara*$^{+/+}$:HCVcpTg mice at 24 months of age. (**A**) Liver-to-body-weight ratio. Results are expressed as the mean ± SD (n = 6/group). (**B**) Numbers of proliferating hepatocytes. Two thousand hepatocytes were examined in each mouse, and hepatocyte nuclei positive for anti-PCNA antibody were counted. Results are expressed as the mean ± SD (n = 6/group). For **A** and **B**, comparisons are designated as follows: *$P < 0.05$ compared with *Ppara*$^{+/+}$ nontransgenic mice; **$P < 0.05$ compared with *Ppara*$^{+/-}$:HCVcpTg mice; #$P < 0.05$ compared with *Ppara*$^{-/-}$:HCVcpTg mice. (**C**) Numbers of apoptotic hepatocytes. Liver sections were subjected to TUNEL staining, and TUNEL-positive hepatocyte nuclei were counted in 2,000 hepatocytes from each mouse. Results are expressed as the mean ± SD (n = 6/group). (**D**) Caspase 3 activity. Results are expressed as the mean ± SD (n = 6/group). (**E**) Immunoblot analysis of oncogene products and cell cycle regulators. The same sample used in Figure 1A (whole-liver lysate, 50 μg protein) was loaded in each well. The band of actin was used as the loading control. Results are representative of 4 independent experiments. The band intensity was quantified densitometrically, normalized by that of actin, and subsequently normalized by that in *Ppara*$^{+/+}$ nontransgenic mice. The mean value of the fold changes is expressed under each band. (**F**) Immunoblot analysis of phosphorylated ERK1/2 and total ERK1/2. The same samples in Figure 4E (50 μg protein) were used.

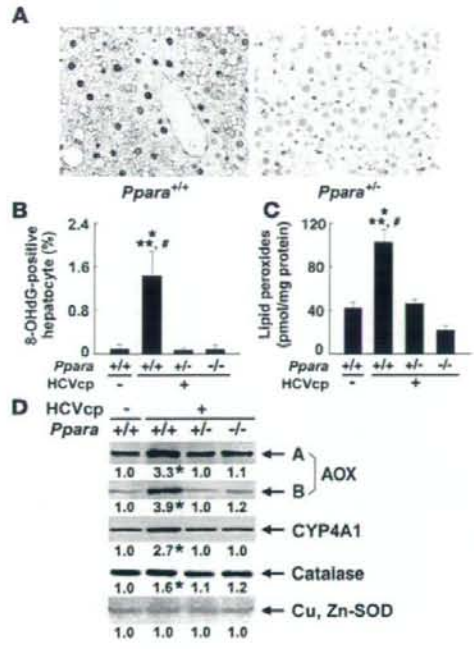

Figure 5
Increased oxidative stress and DNA damage in *Ppara*$^{+/+}$:HCVcpTg mice at 24 months of age. (**A**) Immunohistochemical staining using antibody against 8-OHdG. In *Ppara*$^{+/+}$:HCVcpTg mice, some steatotic hepatocytes were positive for 8-OHdG. Original magnification, ×400. (**B**) Numbers of 8-OHdG–positive hepatocytes. Hepatocyte nuclei stained with anti-8-OHdG antibody were counted in 2,000 hepatocytes of each mouse. Results are expressed as the mean ± SD (n = 6/group). (**C**) Hepatic content of lipid peroxides. Results are expressed as the mean ± SD (n = 6 /group). $^{*}P < 0.05$ compared with *Ppara*$^{+/+}$ nontransgenic mice; $^{**}P < 0.05$ compared with *Ppara*$^{+/-}$:HCVcpTg mice; $^{\#}P < 0.05$ compared with *Ppara*$^{-/-}$:HCVcpTg mice. (**D**) Immunoblot analysis of AOX, CYP4A1, catalase, and Cu, Zn-SOD. The whole-liver lysate used in the experiment in Figure 4E (20 μg protein for AOX and CYP4A1 and 50 μg for others) was loaded in each lane. The band of actin was used as the loading control. Results are representative of 4 independent experiments. **A** and **B** indicate full-length and truncated AOX, respectively. The band intensity was quantified densitometrically, normalized by that of actin, and subsequently normalized by that in *Ppara*$^{+/+}$ nontransgenic mice. The mean value of the fold changes is expressed under each band. $^{*}P < 0.05$ compared with *Ppara*$^{+/+}$ nontransgenic mice.

function. The number of hepatocytes positive for 8-hydroxy-2′-deoxyguanosine (8-OHdG), an indicator of oxidative damage to nuclear DNA, was increased only in 24-month-old *Ppara*$^{+/+}$:HCVcpTg mice (Figure 5, A and B). Lipid peroxides were slightly increased in the livers of 9-month-old *Ppara*$^{+/+}$:HCVcpTg mice (data not shown) and were more abundant in the livers of 24-month-old *Ppara*$^{+/+}$:HCVcpTg mice than in those of *Ppara*$^{+/-}$:HCVcpTg and *Ppara*$^{-/-}$:HCVcpTg mice or *Ppara*$^{+/+}$ nontransgenic mice (Figure 5C). Expression of typical ROS-generating enzymes (AOX and cytochrome P450 4A1 [CYP4A1]) and ROS-eliminating enzymes (catalase and Cu, Zn-SOD) was examined. Immunoblot analysis showed marked increases in the expression of AOX and CYP4A1 and mild increases in that of catalase only in *Ppara*$^{+/+}$:HCVcpTg mice. No changes in Cu, Zn-SOD were found in the subgroups of transgenic mice (Figure 5D). These results suggest that enhanced oxidative stress causes damage in nuclear DNA and probably in mitochondria in the *Ppara*$^{+/+}$:HCVcpTg mice.

Persistent and spontaneous PPARα activation in Ppara$^{+/+}$*:HCVcpTg mice.* Liver tumorigenesis induced by long-term exposure to peroxisome proliferators and the related changes, such as sustained hepatocyte proliferation and increased oxidative stress, are associated with persistent PPARα activation (19–21). To examine the activation of PPARα, we quantified the level of PPARα mRNA, which is induced by PPARα activation (24, 25). PPARα mRNA levels were higher in 9-month-old *Ppara*$^{+/+}$:HCVcpTg mice than in *Ppara*$^{+/+}$ nontransgenic mice (Figure 6A). These increases were more pronounced at 24 months of age. However, there were no differences in PPARα mRNA levels between *Ppara*$^{+/-}$:HCVcpTg and *Ppara*$^{+/-}$ nontransgenic mice at either 9 or 24 months of age. The expression levels of typical PPARα target genes (16, 25, 26) — such as FAT, FATP, L-FABP, AOX, and MCAD (Figure 2); c-Myc, cyclin D1, CDK4, and PCNA (Figure 4); and CYP4A1 (Figure 5) — were simultaneously and synchronously increased in *Ppara*$^{+/+}$:HCVcpTg mice, but not in *Ppara*$^{+/-}$:HCVcpTg or *Ppara*$^{-/-}$:HCVcpTg mice. These results confirm that persistent activation of PPARα occurs only in *Ppara*$^{+/+}$:HCVcpTg mice. Various changes observed in *Ppara*$^{+/+}$:HCVcpTg mice, i.e., increased fatty acid uptake, mitochondrial abnormalities, steatosis, ROS overproduction, accelerated hepatocyte proliferation, and hepatocarcinogenesis, were considered to be closely linked with sustained PPARα activation.

Nuclear PPARα content. The results described above suggest that persistent PPARα activation is critical to the steatogenesis and hepatocarcinogenesis induced by the HCV core protein. A question arises as to why *Ppara*$^{+/+}$:HCVcpTg mice with an active *Ppara* allele do not exhibit the hallmarks of PPARα activation and do not develop HCC. To address this issue, the nuclear PPARα content was analyzed. Immunoblot analysis for PPARα showed that the amount of nuclear PPARα protein in *Ppara*$^{+/+}$:HCVcpTg mice was approximately 2- to 3-fold that of *Ppara*$^{+/+}$ nontransgenic mice, which was disproportionate to the higher PPARα mRNA levels (approximately 1.2- to 1.6-fold) (Figure 6, A and B). The level of nuclear PPARα in *Ppara*$^{+/-}$:HCVcpTg mice was significantly lower than that in *Ppara*$^{+/+}$:HCVcpTg mice and was similar to that in *Ppara*$^{+/+}$ nontransgenic mice (Figure 6B). Thus, the lower amount of nuclear PPARα in *Ppara*$^{+/-}$:HCVcpTg mice than in *Ppara*$^{+/+}$:HCVcpTg mice might have heightened the threshold of expression required for long-term spontaneous PPARα activation.

The degree of an increase in nuclear PPARα levels was evidently higher than the degree of an increase in PPARα mRNA levels in HCVcpTg mice (Figure 6, A and B). To investigate this disparity, the stability of nuclear PPARα was evaluated by pulse-chase experiments using isolated hepatocytes obtained from these mice. The half-life of nuclear PPARα was significantly longer ($P < 0.05$) in *Ppara*$^{+/+}$:HCVcpTg mice (11.5 ± 2.3 h) than in *Ppara*$^{+/+}$ nontransgenic mice (5.8 ± 1.4 h) (Figure 6C). The half-life of nuclear PPARα in *Ppara*$^{+/-}$:HCVcpTg mice tended to be prolonged compared with that in *Ppara*$^{+/-}$ nontransgenic mice (Figure 6C). These results suggest that the stability of nuclear PPARα was increased as a result of HCV core protein expression. Because it is known that the core protein interacts with retinoid X receptor α (RXRα) (27) and that

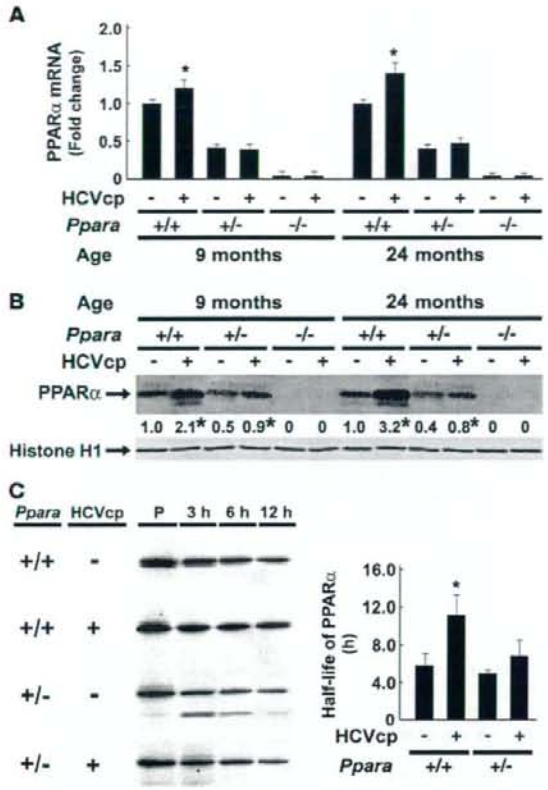

Figure 6

Persistent PPARα activation in *Ppara*$^{+/+}$:HCVcpTg mice. (**A**) PPARα mRNA levels. Total RNA was prepared from each mouse, and PPARα mRNA levels were determined by RT-PCR, normalized by those of GAPDH, and subsequently normalized by those of 9-month-old *Ppara*$^{+/+}$ nontransgenic mice. Results are expressed as the mean ± SD (n = 6 /group). (**B**) Immunoblot analysis of nuclear PPARα. The nuclear fraction obtained from each mouse (100 μg protein) was loaded in each well. The band of histone H1 was used as the loading control. Results are representative of 6 independent experiments. The band intensity was quantified densitometrically, normalized by that of histone H1, and subsequently normalized by that in 9-month-old *Ppara*$^{+/+}$ nontransgenic mice. The mean value is expressed under each band. *P < 0.05 compared with nontransgenic mice of the same age and *Ppara* genotype. (**C**) Pulse-chase experiments for 3, 6, and 12 h and pulse-label (P) experiments for nuclear PPARα using isolated mouse hepatocytes. Left: labeled PPARα bands on x-ray film. Pulse-label and pulse-chase experiments were performed as described in Methods. Results are representative of 4 independent experiments. Right: half-life of PPARα. The band intensity was measured densitometrically and subsequently normalized by that of the pulse-label experiments. The percentage of the band intensity was plotted, and the half-life of PPARα was calculated. Results obtained from 4 independent experiments are expressed as the mean ± SD. *P < 0.05 compared with nontransgenic mice in the same *Ppara* genotype.

PPARα influences the stability of RXRα (28), it is plausible that the core protein would affect its action in nuclei through an interaction with the PPARα-RXRα heterodimer and stabilization of PPARα.

Development of hepatic steatosis and HCC with long-term clofibrate treatment in Ppara$^{+/-}$*:HCVcpTg mice.* To further confirm the significance of persistent PPARα activation on core protein–induced pathological changes, *Ppara*$^{+/-}$ and *Ppara*$^{+/-}$:HCVcpTg mice were fed a standard diet containing 0.05% clofibrate for 24 months. Interestingly, hepatic steatosis appeared in the clofibrate-treated *Ppara*$^{+/-}$:HCVcpTg mice, but not in the *Ppara*$^{+/-}$ mice under the same treatment conditions (Figure 7, A and B). Similar to our observations in *Ppara*$^{+/+}$:HCVcpTg mice not treated with clofibrate, aberrant mitochondria with discontinuous outer membranes and decreased palmitic acid β-oxidation activity were found only in the clofibrate-treated *Ppara*$^{+/-}$:HCVcpTg mice (Figure 7, A and C). In addition, levels of MCAD mRNA; AOX, and CYP4A1 proteins; PPARα mRNA; and nuclear PPARα protein were higher in the clofibrate-treated *Ppara*$^{+/-}$:HCVcpTg mice than in the clofibrate-treated *Ppara*$^{+/-}$ mice (Figure 7, D–F), which suggests that the degree of PPARα activation in the former group was greater than that in the latter group and similar to that in *Ppara*$^{+/+}$:HCVcpTg mice not treated with clofibrate. Finally, the incidence of HCC after clofibrate treatment was higher in *Ppara*$^{+/-}$:HCVcpTg mice (25%; 5 in 20 mice) than in *Ppara*$^{+/-}$ mice (5%; 1 in 20 mice). Therefore, these results corroborate the importance of constant PPARα activation to the pathogenesis of hepatic steatosis and HCC in the transgenic mice.

Discussion

A novel and striking finding in this study is the absolute requirement of persistent PPARα activation for the development of HCV core protein–induced steatosis and HCC. Our data also show that the HCV core protein alone cannot induce steatosis and HCC in transgenic mice.

Mechanisms of development of steatosis in HCVcpTg mice were previously explained as an enhancement of de novo synthesis of fatty acids (29) and a decrease in MTP expression, the latter of which results in insufficient VLDL secretion from hepatocytes (30). In the present study, we revealed 2 novel mechanisms of steatogenesis in the transgenic mice, i.e., an impairment of mitochondrial β-oxidation due to the breakdown of mitochondrial outer membranes and an increase in fatty acid uptake into hepatocytes, associated with PPARα activation. PPARα activation, mitochondrial dysfunction, and hepatic steatosis appeared in 9-month-old *Ppara*$^{+/+}$:HCVcpTg mice and continued until 24 months of age, clearly preceding development of HCC. These findings thereby indicate a correlation between PPARα activation, hepatic steatosis, and HCC.

We obtained the novel and rather paradoxical finding that significant PPARα activation, which generally is expected to reduce hepatic triglyceride levels, is essential for the development of severe steatosis induced by HCV core protein. According to the results of this study, the following hypothesis concerning the development of steatosis in *Ppara*$^{+/+}$:HCVcpTg mice is proposed. First, the HCV core protein localizes partly in mitochondria (9). A recent study

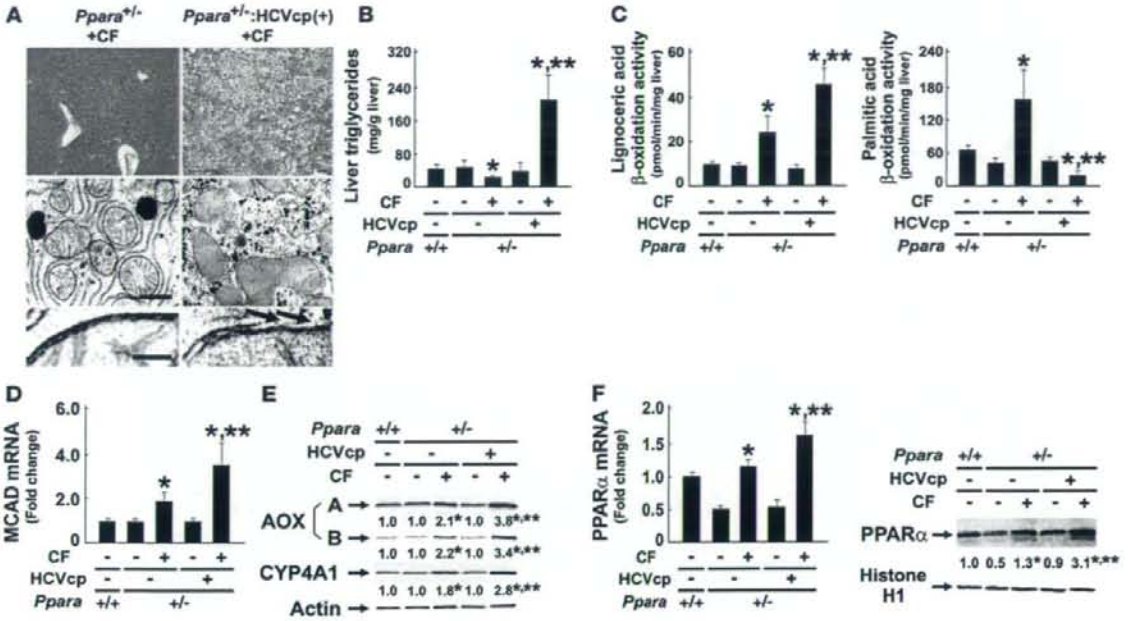

Figure 7

Development of hepatic steatosis by long-term treatment of clofibrate in *Ppara*$^{+/-}$:HCVcpTg mice. (**A**) Histological examination of *Ppara*$^{+/-}$ and *Ppara*$^{+/-}$:HCVcpTg mice treated with diet containing 0.05% (w/w) clofibrate for 24 months (CF). Top: Histological appearance of H&E-stained liver sections. Magnification, ×40. Microvesicular and macrovesicular steatosis were detected only in clofibrate-treated *Ppara*$^{+/-}$:HCVcpTg mice. Middle and bottom: Electron microscopic features of hepatic mitochondria. Some C-shaped mitochondria showing discontinuance of outer membranes (arrows) were found in clofibrate-treated *Ppara*$^{+/-}$:HCVcpTg mice. Scale bars: 400 nm (middle), 30 nm (bottom). (**B** and **C**) Content of liver triglycerides and lignoceric and palmitic acid β-oxidation activities. (**D**) MCAD mRNA levels. mRNA levels were normalized to those of GAPDH and subsequently normalized to those in *Ppara*$^{+/+}$ nontransgenic mice. (**E**) Immunoblot analysis of AOX and CYP4A1. Whole-liver lysate (20 μg protein) was loaded in each lane. Actin was used as a loading control. Results are representative of 6 independent experiments. (**F**) PPARα mRNA levels and nuclear PPARα contents. Left: PPARα mRNA levels. The same samples used in **D** were adopted. Right: Immunoblot analysis of nuclear PPARα. Nuclear fraction obtained from each mouse (100 μg protein) was loaded in each well. Histone H1 was used as a loading control. In **E** and **F**, the mean value of the fold changes is shown under each band. Results are representative of 6 independent experiments. Band intensity was quantified densitometrically, normalized to that of the loading control, and subsequently normalized to that in *Ppara*$^{+/+}$ nontransgenic mice. *$P < 0.05$ compared with untreated mice of the same genotype; **$P < 0.05$ compared with clofibrate-treated *Ppara*$^{+/-}$ mice without core protein gene. Results are expressed as mean ± SD (n = 6/group).

showed that, in isolated mitochondria, the core protein directly increased Ca^{2+} influx, inhibited electron transport complex I activity, and induced ROS production (31), all of which can increase the fragility of mitochondria and depress mitochondrial function. In addition, the HCV core protein also localizes in nuclei (9) and can coexist in PPARα-RXRα heterodimer through a direct interaction with the DNA-binding domain of RXRα, which enhances the transcriptional activity of PPARα target genes, such as AOX, despite the absence of PPARα ligands in cultured cells (27). The HCV core protein can also be involved in the PPARα-RXRα complex through a direct interaction with cyclic-AMP responsive element binding protein-binding protein (32), which is able to bind to PPARα (33). Thus, the core protein probably serves as a coactivator and stabilizer of PPARα in vivo, which was further confirmed in this study. Moreover, because it is also known that the core protein itself activates ERK1/2 and p38 mitogen-activated protein kinase (34), these activations might phosphorylate PPARα and thereby transactivate it (35). The core protein–induced PPARα activation enhances the basal expression of AOX and CYP4A1, which leads to increased production of ROS and dicarboxylic acids. These toxic compounds can damage mitochondrial outer membranes, which impairs the mitochondrial β-oxidation system. These damages directly induce the accumulation of long-chain fatty acids in hepatocytes. Furthermore, PPARα activation increases the expression of FAT and FATP, which promotes the influx of fatty acids from blood. Long-chain fatty acids and their CoA esters accumulated in hepatocytes are likely to act as potent detergents, which further damages the outer membranes of mitochondria. Fatty acids and their derivatives function as natural ligands of PPARα, which results in the activation of PPARα and the induction of FAT, FATP, AOX, and CYP4A1, which further accelerates mitochondrial damage, the reduction of mitochondrial β-oxidation activity, and the accumulation of fatty acids in a vicious cycle.

Persistent PPARα activation increases oxidative DNA damage because of a disproportionate increase in ROS-generating enzymes relative to the levels of degrading enzymes such as catalase and SOD, which can predispose hepatocytes to malignant transformation. In addition, persistent PPARα activation leads to increased

Table 2
Primer pairs used for RT-PCR

Gene	GeneBank accession number		Primer sequence	Product (bp)
ACC	NM_133360	F	5′-GGGCACAGACCGTGGTAGTT-3′	105
		R	5′-CAGGATCAGCTGGGATACTGAGT-3′	
ApoB	NM_009693	F	5′-TCACCCCCGGGATCAAG-3′	85
		R	5′-TCCAAGGACACAGAGGGCTTT-3′	
AOX	NM_015729	F	5′-TGGTATGGTGTCGTACTTGAATGAC-3′	145
		R	5′-AATTTCTACCAATCTGGCTGCAC-3′	
FAS	NM_007988	F	5′-ATCCTGGAACGAGAACACGATCT-3′	140
		R	5′-AGAGACGTGTCACTCCTGGACTT-3′	
FAT	NM_007643	F	5′-CCAAATGAAGATGAGCATAGGACAT-3′	87
		R	5′-GTTGACCTGCAGTCGTTTTGC-3′	
FATP	NM_011977	F	5′-ACCACCGGGCTTCCTAAGG-3′	80
		R	5′-CTGTAGGAATGGTGGCCAAAG-3′	
GAPDH	M32599	F	5′-TGCACCACCAACTGCTTAG-3′	177
		R	5′-GGATGCAGGGATGATGTTCTG-3′	
L-FABP	NM_017399	F	5′-GCAGAGCCAGGAGAACTTTGAG-3′	121
		R	5′-TTTGATTTTCTTCCCTTCATGCA-3′	
MCAD	NM_007382	F	5′-TGCTTTTGATAGAACCAGACCTACAGT-3′	128
		R	5′-CTTGGTGCTCCACTAGCAGCTT-3′	
MTP	NM_008642	F	5′-GAGCGGTCTGGATTTACAACG-3′	72
		R	5′-GTAGGTAGTGACAGATGTGGCTTTTG-3′	
PPARα	NM_011144	F	5′-CCTCAGGGTACCACTACGGAGT-3′	69
		R	5′-GCCGAATAGTTCGCCGAA-3′	

F, forward sequence; R, reverse sequence.

cell division, as revealed by the expression of cell cycle regulators such as cyclin D1 and CDK4. Furthermore, there is little change in apoptosis, which, under normal circumstances, would remove damaged cells capable of undergoing transformation. Thus, under these conditions, it is plausible that some aberrant hepatocytes do not undergo apoptosis and develop into HCC.

It is well known that chronic activation of PPARα is associated with hepatocarcinogenesis in mice exposed to peroxisome proliferators or in mice lacking AOX expression. The common clinicopathological characteristics of HCC in these mice are multicentric HCC (20, 22, 36, 37), the well-differentiated appearance of HCC including trabecular features and often a "nodule-in-nodule" pattern (22, 36, 37), and no evidence of fibrosis or cirrhosis in the nonneoplastic liver parenchyma (22, 36), similar to that observed in *Ppara*$^{+/+}$:HCVcpTg mice. However, mice chronically exposed to peroxisome proliferators are clearly distinct from *Ppara*$^{+/+}$:HCVcpTg mice in that they have normal mitochondrial organization, increased mitochondrial β-oxidation activity, and no steatosis (16, 36). AOX-null mice are also different from *Ppara*$^{+/+}$:HCVcpTg mice with respect to mitochondrial structure (22). These detailed comparisons between the 3 mouse models reveal the importance of mitochondrial abnormalities in the pathogenesis of HCV-related diseases.

PPARα is known to regulate the hepatic expression of many proteins associated with fatty acid and triglyceride metabolism, cell division and apoptosis, oxidative stress generation and degradation, and so forth (15, 16, 20, 21, 24–26); therefore, complete deletion of the PPARα gene from mice might cause hitherto unknown influences on the pathways involved in the development of hepatic steatosis and HCC. To consider these unknown effects, *Ppara*$^{+/-}$:HCVcpTg mice were adopted in the current study. Surprisingly, almost all results from *Ppara*$^{+/-}$:HCVcpTg mice were similar to those from *Ppara*$^{-/-}$:HCVcpTg mice, which demonstrates that the presence of functional PPARα itself is not a prerequisite for the occurrence of steatosis and HCC induced by the HCV core protein. Moreover, a comparison between *Ppara*$^{+/-}$:HCVcpTg and *Ppara*$^{+/+}$:HCVcpTg mice uncovered an unexpected and important fact that the core protein–dependent pathological changes do not appear without significant activation of PPARα. Thus, it is not the presence of PPARα per se, but rather a high level of PPARα activation that seems to be essential for the development of HCV core protein–induced steatosis and HCC.

To reinforce the abovementioned hypothesis, *Ppara*$^{+/-}$ and *Ppara*$^{+/-}$:HCVcpTg mice were treated with an exogenous PPAR agonist, clofibrate, for 24 months. In *Ppara*$^{+/-}$ mice, long-term clofibrate treatment caused a certain level of persistent PPARα activation and a low incidence of HCC. Interestingly, in *Ppara*$^{+/-}$:HCVcpTg mice, clofibrate treatment induced more intensive PPARα activation and HCC at a much higher incidence, accompanied by damaged mitochondrial outer membranes, severe steatosis, and decreased mitochondrial β-oxidation activity. The results from the clofibrate-treated *Ppara*$^{+/-}$:HCVcpTg mice were similar to those of the *Ppara*$^{+/+}$:HCVcpTg mice not treated with clofibrate. Therefore, these findings further support the concept that a long-term and high level of PPARα activation is necessary for steatogenesis and hepatocarcinogenesis in HCVcpTg mice and emphasize the significant role of the HCV core protein as a PPARα coactivator in vivo.

A pulse-chase experiment showed that PPARα was stabilized in hepatocyte nuclei in mice expressing the HCV core protein. Many nuclear receptors, including PPARα and RXRα, are known to be degraded by the ubiquitin-proteasome system (38), which plays an important role in modulating the activity of nuclear receptors. Further studies will be needed to clarify whether the core protein influences the ubiquitin-proteasome pathway.

Recent studies have shown conflicting result, i.e., that PPARα was downregulated in the livers of chronic hepatitis C patients (39, 40). Although the association between PPARα function and chronic HCV infection remains a matter of controversy in humans, the changes observed in the transgenic mice resemble in many ways the clinicopathological features of chronically HCV-infected patients; both show a high frequency of accompanying steatosis (10, 40, 41), increased accumulation of carbon 18 monounsaturated fatty acids in the liver (42), mitochondrial dysfunction (43), increased insulin resistance (44) and oxidative stress (45, 46), male-preferential (2) and multicentric occurrence of HCC (47, 48), and the well-differentiated appearance of HCC, including trabecular features and often a "nodule-in-nodule" pattern (47, 48). Thus, it is postulated that the mechanism of steatogenesis and hepatocarcinogenesis we proposed may partially apply to patients with chronic HCV infection. If so, therapeutic interventions to alleviate persistent and excessive PPARα activation might be beneficial in the prevention of HCC. To clarify the exact relationship between PPARα activation and HCV-induced hepatocarcinogenesis in humans, further

experiments using noncancerous liver tissues obtained from HCV-related HCC patients and using mice carrying human PPARα and HCV core protein genes are needed.

In conclusion, we clarified for the first time that persistent and potent PPARα activation is absolutely required for the development of severe steatosis and HCC induced by HCV core protein. In addition, we uncovered paradoxical and specific functions of PPARα in the mechanism of steatogenesis mediated by the core protein. Our results offer clues in the search for novel therapeutic and nutritional management options, especially with respect to neutral lipids, for chronically HCV-infected patients.

Methods

Mice. The generation of HCVcpTg mice and *Ppara*$^{-/-}$ mice was described previously (7, 24, 49). Male HCVcpTg mice and female *Ppara*$^{-/-}$ mice were mated, and F1 mice bearing the HCV core protein gene were intercrossed to produce F2 mice. *Ppara*$^{+/+}$, *Ppara*$^{+/-}$, and *Ppara*$^{-/-}$ mice bearing the HCV core protein gene, designated as *Ppara*$^{+/+}$:HCVcpTg, *Ppara*$^{+/-}$:HCVcpTg, and *Ppara*$^{-/-}$:HCVcpTg mice, in the F4 generation were subjected to serial analyses. Because HCC develops preferentially in male HCVcpTg mice (9), male mice were analyzed. Age-matched male *Ppara*$^{+/+}$ mice without the core protein gene were used as controls. For identifying genotypes, genomic DNA was isolated from mouse tails and amplified by PCR. Primer pairs were designed as described elsewhere: 5′-GCCCACAGGACGTTAAGTTC-3′ and 5′-TAGTTCACGCCGTCCTCCAG-3′ for the HCV core gene (7) and 5′-CAGAGCAACCATCCAGATGA-3′ and 5′-AAACGCAACGTAGAGTGCTG-3′ for the PPARα gene (24). Amplified alleles for HCV core and PPARα genes were 460 and 472 base pairs, respectively. Five mice per cage were fed a routine diet and were kept free of specific pathogens according to institutional guidelines. For the clofibrate treatment experiments, 2-month-old male *Ppara*$^{+/-}$ and *Ppara*$^{+/-}$:HCVcpTg mice were randomly divided into 2 groups (n = 20 in each group) and were fed either a routine diet or one containing 0.05% (w/w) clofibrate (Wako Pure Chemicals Industries) for 24 months. All mice were killed by cervical dislocation before their livers were excised. If a hepatic tumor was present, the tumor was removed and subjected to histological analysis, and the remaining liver tissues were used for biochemical analyses. All animal experiments were conducted in accordance with animal study protocols outlined in the *Guide for the Care and Use of Laboratory Animals* prepared by the National Academy of Sciences and approved by the Shinshu University School of Medicine.

Preparation of nuclear, mitochondrial, and cytosolic fractions. Approximately 400 mg of liver tissue was minced on ice and transferred to 10% (w/v) isolation buffer (250 mM sucrose in 10 mM Tris-HCl [pH 7.4] and 0.5 mM EGTA and 0.1% bovine serum albumin [pH 7.4]). The samples were gently homogenized by 10–20 strokes with a chilled Dounce homogenizer (Wheaton) and loose-fitting pestle. The homogenate was centrifuged at 500 × *g* for 5 min at 4°C. The supernatant was retained, and the resulting pellet was resuspended with isolation buffer and centrifuged at 4,500 *g* for 10 min at 4°C. The pellet fraction was suspended again and centrifuged at 20,000 × *g* for 1 h at 4°C, and the resulting pellet was used as the nuclear fraction. The combined supernatant fractions were centrifuged at 7,800 × *g* for 10 min at 4°C to obtain a crude mitochondria pellet. This pellet was resuspended with isolation buffer, centrifuged at 7,800 × *g* for 10 min at 4°C, and used as the mitochondrial fraction. Finally, all supernatant fractions were collected and centrifuged at 20,000 × *g* for 30 min at 4°C, and the resulting supernatant was used as the cytosolic fraction.

Immunoblot analysis. Protein concentrations were measured colorimetrically with a BCA Protein Assay kit (Pierce). For the analysis of fatty acid–metabolizing enzymes, hepatocyte mitochondrial fractions or whole-liver lysates (20 μg protein) were subjected to 10% SDS-PAGE (16). For analysis of PPARα, nuclear fractions (100 μg protein) were used. For analysis of other proteins, whole lysates or cytosolic fractions (50 μg protein) were subjected to electrophoresis. After electrophoresis, the proteins were transferred to nitrocellulose membranes, which were incubated with the primary antibody and then with alkaline phosphatase–conjugated goat anti-rabbit or anti-mouse IgG. Antibodies against HCV core protein, fatty acid–metabolizing enzymes, CYP4A1, catalase, and PPARα were described previously (9, 16, 24, 50). Antibodies against other proteins were purchased commercially: cytochrome *c* antibody from BD Transduction Laboratories and other antibodies from Santa Cruz Biotechnology. The band of actin or histone H1 was used as the loading control. The band intensity was measured densitometrically, normalized to that of actin or histone H1, and subsequently expressed as fold changes relative to that of *Ppara*$^{+/+}$ nontransgenic mice.

Analysis of mRNA. Total liver RNA was extracted using an RNeasy Mini Kit (Qiagen), and cDNA was generated by SuperScript II reverse transcriptase (Gibco BRL). Quantitative RT-PCR was performed using a SYBR green PCR kit and an ABI Prism 7700 Sequence Detection System (Applied Biosystems). The primer pairs used for RT-PCR are shown in Table 2. The mRNA level was normalized to the GAPDH mRNA level and subsequently expressed as fold changes relative to that of *Ppara*$^{+/+}$ nontransgenic mice.

Light microscopy and immunohistochemical analysis. Small blocks of liver tissue from each mouse were fixed in 10% formalin in phosphate-buffered saline and embedded in paraffin. Sections (4 μm thick) were stained with hematoxylin and eosin. For immunohistochemical localization of PCNA and 8-OHdG, other small blocks of liver tissue were fixed in 4% paraformaldehyde in phosphate-buffered saline. Sections (4 μm thick) then were affixed to glass slides and incubated overnight with mouse monoclonal antibodies against PCNA (1:100 dilution; Santa Cruz) or 8-OHdG (1:10 dilution; Japan Institute for the Control of Aging). Sections were immunostained using EnVision+ kit, with 3,3′-diaminobenzidine as a substrate (DAKO). Hepatocytes positive for PCNA or 8-OHdG were examined in 10 randomly selected ×400 microscopic fields per section. Two-thousand hepatocytes were examined for each mouse, and the number of immunostained hepatocyte nuclei was expressed as a percentage.

Assessment of hepatocyte apoptosis. TUNEL assay was performed using a MEBSTAIN Apoptosis Kit II (Medical & Biological Laboratories). Two thousand hepatocytes were examined for each mouse, and the number of TUNEL-positive hepatocytes was expressed as a percentage.

Pulse-label and pulse-chase experiments. Parenchymal hepatocytes were isolated by the modified *in situ* perfusion method (51). After perfusion with 0.05% collagenase solution (Wako), the isolated hepatocytes were washed 3 times by means of differential centrifugation and the dead cells were removed by density-gradient centrifugation at 500 *g* for 3 min at 4°C on Percoll (Amersham Pharmacia Biotech). The live hepatocytes were washed and suspended in William's E medium containing 5% FBS. When the viability of the isolated hepatocytes exceeded 85% as determined by the trypan blue exclusion test, the following experiments were conducted. The isolated hepatocytes were washed twice and incubated in methionine-free medium containing 5% dialyzed FBS for 1 h at 37°C. The medium was replaced with the same medium containing 300 mCi/ml of [^{35}S]methionine (Amersham Pharmacia Biotech). After a 3-h incubation, the labeled medium was exchanged for the standard medium, and the preparation was chased for 3, 6, or 12 h. The labeled cells were washed, homogenized, and centrifuged at 800 *g* for 5 min at 4°C to obtain a crude nucleus pellet. This pellet was resuspended with isolation buffer and centrifuged at 20,000 *g* for 1 h at 4°C to prepare the nuclear fraction. The levels of radioactivity in the homogenates of the pulse-labeled preparations were similar between the transgenic and the nontransgenic mice, which suggested that the [^{35}S]methionine uptake capacity in the former hepatocytes was similar to that in the latter. The nuclear fraction was lysed in RIPA buffer (10 mM Tris-HCl, pH 7.4; 0.2% sodium deoxycholate, 0.2% Nonidet P-40, 0.1% SDS,